ZRNIC'

DRAFT

DOPPLER RADAR DUAL POLARIZATION CONSIDERATIONS FOR NEXRAD

Dale Sirmans, Dusan Zrnic', Mangalore Sachidananda

National Severe Storms Laboratory
National Oceanic and Atmospheric Administration
Department of Commerce
1313 Halley Circle
Norman, Oklahoma 73069

October 1984

Revised July 1986

Prepared for

JOINT SYSTEMS PROGRAMS OFFICE
National Weather Service
National Oceanic and Atmospheric Administration
Department of Commerce
Rockville, Maryland

Doppler Radar Dual Polarization
Considerations for NEXRAD

Appendix: Simultaneous Dual Polarization Measurements

A.1) Z_{DR} measurement criteria compatible with NEXRAD

A.2) Z_{DR} measurement with simultaneous sampling

1. INTRODUCTION

In formulating technical requirements for the Next Generation Weather Radar (NEXRAD), several features which would enhance the system capability were considered although they were not required for the prime mission of the system. Dual polarization has been recognized as a potential method for improving certain meteorological measurements by radar and was among the adjunct features considered but deleted from initial requirements.

In the following report we re-examine the dual polarization in light of recent work in both meteorological measurements using this method and the engineering technology necessary to support it.

It should be noted that a key word in the assessment is the potential benefit. Dual polarization and the associated fundamental measurement, differential reflectivity, i.e., the ratio (in dB) of apparent radar cross section at orthogonal polarizations, is not an operationally established technique with proven meteorological measurement capability. However, the work to date and primary results of ongoing research are encouraging and it is not premature to consider the technique at this time especially since the measurement techniques are becoming well defined and the hardware performance well established. The data base for evaluation is limited but most of the fundamental work necessary to validate the concepts behind the scheme has been done. It is not anticipated that any significant changes in either physical interpretation or statistical properties will result from future studies.

The possible meteorological benefits to NEXRAD are assessed and the impact on the baseline system prime mission are examined. Possible compromises in existing NEXRAD capability necessary to accommodate the dual polarization measurement outlined. A new approach requiring substantial engineering development appears to be the only way dual polarization could be incorporated into the NEXRAD without serious compromise of the prime mission.

This report is intended to serve as a source of information for NEXRAD program policy decision. An effort is made to provide the pertinent information but in most cases results are presented without rigorous derivation.

2. DUAL POLARIZATION METHOD

2.1. Theoretical information contained in the measurement

Doppler radar with single polarized transmission provides estimates of the first three spectral moments. These estimates contain information about the radar scatterers in terms of reflectivity factor, velocity and velocity variance in the radar sample volume. While these spectral moments provide a great deal of information they do not characterize a meteorological field completely. Certain parameters related to precipitation rate, such as median volume drop diameter, and thermodynamic phase state, cannot be determined accurately from reflectivity measurement alone.

Study of the polarization dependent scatter properties of hydrometeors has led to the use of dual polarization in radars to extract additional information about the scatterers. Though the reported measurements using dual polarization method are confined to differential reflectivity (Z_{DR}) and linear depolarization ratio (LDR) in the case of linear polarization and circular depolarization ratio (CDR) in the case of circular polarization, the results have indicated the potential usefulness of these measurements for improving the accuracy of precipitation rate estimation. There have been efforts to identify the phase state of the precipitation using Z_{DR} data and although preliminary results are encouraging the database is still too small for determining the statistical significance of these results.

In this section we examine the polarization properties of hydrometeors in order to assess how much additional information we can derive by implementing polarization diversity in a Doppler radar. In practice there are two types of polarization measurements - linear polarization and circular polarization. When a complete scattering matrix is evaluated the information content of the two measurements is the same. In this case a set of measurements in linear polarization can be transformed into circular polarization measurements by matrix transformation and vice versa. However, it may not be practical to measure the complete scattering matrix, in which case the partial measurement of polarization properties of the scatterers in the resolution volume does not lead to the same results using linear or circular polarization. Each method has advantages and disadvantages in terms of practical implementation and the derivable information content.

2.1.1 Linear polarization

Consider the electromagnetic field scatter property of a single hydrometeor such as a raindrop, snowflake, hailstone, etc. A monostatic radar such as NEXRAD measures only the backscattered signal, hence, it is sufficient to examine only the backscattered field. The two orthogonal components of the scattered electric field can be expressed in terms of the scattering matrix [S]

$$\begin{matrix} E_H{}^s \\ E_V{}^s \end{matrix} = \begin{matrix} S_{HH} & S_{HV} \\ S_{VH} & S_{VV} \end{matrix} \begin{matrix} E_H{}^i \\ E_V{}^i \end{matrix} \qquad (2.1)$$

where E is the electric field, and the superscripts s, i indicate the scattered and incident field components. S is the scattering coefficient and successive subscripts refer to signal polarizations (H-horizontal, V-vertical) for incident and backscatter. In general the elements of the scattering matrix are complex and are functions of the scatterer shape, size, orientation, and dielectric constant. For an incident field of horizontal polarization ($E_V{}^i = 0$), the scattered field components $E_H{}^s$, $E_V{}^s$ are proportional to the two matrix elements S_{HH} and S_{VH}, while for excitation with a vertically polarized field ($E_H{}^i = 0$) the scattered field components $E_H{}^s$, $E_V{}^s$ are proportional to the matrix elements S_{HV} and S_{VV}.

The radar resolution volume usually consists of a large number of scatterers often of mixed phases so the backscattered field measured by the radar is the vectoral sum of the backscattered field from each of the scatterers. The dimension of the volume is much larger than the wavelength. The scatterers are distributed over the entire volume, have different cross sections and are in motion relative to each other. Thus the phases of the individual scattered field components are random. This makes the received signal statistical, and a number of measurements have to be made in order to estimate the composite of the backscattered power. The information about the scatterer shape, orientation, phase state and size distribution is contained in the scattering matrix (of the resolution volume) and it is possible to extract some of this information using the relative amplitudes of the elements of the scattering matrix. The most useful information is the thermodynamic phase state and the drop size distribution, which are essential for accurate determination of precipitation rate and cloud condition.

To understand how the scattering matrix reflects the scattering properties, let us examine the field scattering matrix of a raindrop. It is well established through numerous studies that a free-falling water drop assumes a shape which can be approximated by an oblate spheroid and at equilibrium (i.e., a drop falling at terminal velocity) the oblateness (or eccentricity) of the spheroid is a function of the drop size.

For the ideal drop orientation relative to the incident electric fields as shown in Figure 2.1a the backscattered field in terms of the horizontal and vertical dipole moments p_h and p_v is given by

$$\begin{matrix} E_H{}^s \\ E_V{}^s \end{matrix} = \begin{matrix} p_h & 0 \\ 0 & p_v \end{matrix} \quad \begin{matrix} E_H{}^i \\ E_V{}^i \end{matrix} \tag{2.2}$$

where

$$p_h = \frac{4\pi ab^2}{3} \varepsilon_o (m^2 - 1) \left[\frac{2}{I(m^2 - 1) + m^2 + 1}\right]$$

$$p_v = \frac{4\pi ab^2}{3} \varepsilon_o (m^2 - 1) \left[\frac{1}{I(m^2 - 1) + 1}\right]$$

$$I = \frac{1}{e^2} [1-(\frac{1}{e^2} - 1)^{1/2} \sin^{-1} e]$$

$e = [1 - (\frac{a}{b})^2]^{1/2}$; eccentricity of the ellipsoid

a/b - axis ratio of raindrop

$m = \sqrt{\varepsilon_r}$ - refractive index

Note that the dipole moments p_h and p_v are functions of the drop geometry, particularly the eccentricity of the ellipsoid as well as the dielectric constant of the drop. Since the eccentricity is a known function of the drop diameter for drops falling at terminal velocity, an estimate of eccentricity provides an estimate of drop diameter.

For the general orientation shown in Figure 2.1b the scattering matrix can be expressed as (Stapor and Pratt, 1984)

$$\begin{matrix} (p_v - p_h)\cos^2\delta\,\sin^2\psi + p_h & \frac{1}{2}(p_v - p_h)\cos^2\delta\sin 2\psi \\ \frac{1}{2}(p_v - p_h)\cos^2\delta\,\sin 2\psi & (p_v - p_h)\cos^2\delta\cos^2\psi + p_h \end{matrix} \qquad (2.3)$$

where

δ = elevation angle of the drop = angle between $\overline{n}$ and x, y plane

ψ - angle measured from y axis to the projection of drop semi minor axis onto the x, y plane,

The dipole moments p_h and p_v, in the major and minor axis direction respectively, are still functions of the geometry of the drop shape and the dielectric constant. All four elements of the scattering matrix are functions of the drop elevation, δ, and orientation, ψ, but the off-diagonal terms are more strongly dependent on ψ. The diagonal terms are proportional to the radar reflectivities for the horizontally and vertically polarized fields and the ratio is a measure of eccentricity of the drop.

Now the resolution volume consists of drops of various sizes with a size distribution $N(D_e)$ and possibly with a canting angle (i.e., the angle between drop major axis and incident horizontal field) distribution about a mean ψ_o. $N(D_e)$ represents the number density of drops as a function of equivolumetric diameter. The scattering matrix measured by the radar (Eq. 2.1) represents the integrated effect of all the scatterers. Raindrops are known to have preferred orientation with their major axis along the horizontal and in most cases the mean canting angle ψ_0 is nearly zero. A two-parameter drop size distribution could be determined using only the diagonal terms of the scattering matrix. The ratio of the diagonal terms, the differential reflectivity Z_{DR}, provides an unbiased estimate of the two parameters of the drop size distribution assuming the mean canting angle to be zero. If $\psi_0 \neq 0$, the value of Z_{DR} is reduced due to cross couplings, and measurement of the off-diagonal terms is necessary to gain information about this mean canting angle.

Another important parameter that can be used to determine accurate drop size distribution (DSD) is the differential propagation phase shift. Because of the oblateness of the raindrops the effective propagation constant for the horizontally polarized electromagnetic field is different from that for the vertically polarized field. Since the transmitted pulse propagates through the meteorological field to the resolution volume and the scattered field propagates back along the same path, the path integrated propagation properties of the intervening medium, in terms of attenuation and phase shift, are contained in the apparent scattering matrix parameters measured by the radar. The differential phase shift can be extracted from the complex voltage samples measured using a dual polarized radar. Measurement of one of the differential parameters, differential reflectivity or differential phase shift constant, in conjunction with horizontal or vertical reflectivity, is sufficient to determine a two parameter DSD. The selection criteria as to which of the two differential parameters is more suitable for NEXRAD is the relative ease of measurement and obtainable accuracies.

One of the potential uses of dual polarization measurements may be in identification of hydrometeor type, i.e., rain, drizzle, cloud, fog, snow, graupel, hail, etc. It may be possible to determine, by theoretical analysis, the approximate range of values of the scattering matrix elements for each of these scatterers. There have been some studies to identify different types of hydrometeors based on differential reflectivity and horizontal reflectivity alone (Bringi and Seliga, 1977; Seliga and Bringi, 1978; Hall **et al.**, 1980). The results to date show that the range of values of Z_H and Z_{DR} often overlaps for different types of hydrometeors and identification may be ambiguous. However, an examination of the complete scattering matrix may provide additional information that can be used to identify the hydrometeor type.

2.1.2 Circular Polarization

The two orthogonal circular polarizations are the right hand circular (RHC) and left hand circular (LHC). If a circularly polarized wave is transmitted, the backscattered wave can be resolved into RHC and LHC components. For a RHC transmission the main component of the backscattered field is in a LHC wave and the cross coupled component is in a RHC wave. The orientation of the minor axis of the polarization ellipse can be estimated from the phase difference between the RHC and LHC waves. (Strictly true only for a monochromatic wave.)

The backscattered signal from precipitation is narrow band Gaussian. This means that the scattered signal contains more than one frequency but the departure from mean frequency is small. The departure from mean frequency is the result of Doppler spread caused by the relative movement of precipitation particles.

As in linear polarized transmission, the circularly polarized signal can be expressed in terms of a scatter matrix [C]

$$\begin{matrix} E_R{}^s \\ E_L{}^s \end{matrix} = \begin{matrix} C_{RR} & C_{RL} \\ C_{LR} & C_{LL} \end{matrix} \quad \begin{matrix} E_R{}^i \\ E_L{}^i \end{matrix} \tag{2.4}$$

where subscripts R and L represent RHC and LHC components. These components can be converted to linear polarized components E_H and E_V by matrix transformation,

$$\begin{matrix} E_R{}^s \\ E_L{}^s \end{matrix} = \frac{1}{\sqrt{2}} \begin{matrix} 1 & j \\ 1 & -j \end{matrix} \quad \begin{matrix} E_H{}^s \\ E_V{}^s \end{matrix} = [U] \begin{matrix} E_H{}^s \\ E_V{}^s \end{matrix} \tag{2.5}$$

where $j = \sqrt{-1}$, and [U] is the transformation matrix. Inverse transformation is done using the transpose of the matrix [U].

Because of the statistical nature of the backscattered signal, measurement from a single pulse will have too large an uncertainty in the scattering matrix to be useful for deriving the information about the scatterers. Using a large number of measurements we can estimate the expected values of the backscattering matrix elements for the resolution volume. Because the individual scattering matrices for circular and linear polarizations contain the same information, the estimated scattering matrices (2.2) of the resolution volume for circular and linear polarization will also contain the same information. But individual matrix terms and derived quantities from these terms are affected differently by the polarization properties of the scatterers. For example, the ratio $(\frac{C_{RL}}{C_{RR}})^2$ known as the circular depolarization ratio (CDR), obtained using only RHC transmission, is independent of mean canting angle but is affected by the distribution of canting angles. The corresponding parameter Z_{DR} from horizontally and vertically polarized transmissions is affected by mean canting angle. Differential propagation severely affects CDR while Z_{DR} is nearly unaffected if horizontal and vertical transmissions are made alternately.

2.2 Measurable Quantities From Established Techniques

Technology exists for the measurement of the complete scatter matrix in linear and circular polarized transmission. However, because of the statistical nature of signals and the propagation effect present in the measurements, we need to assess the accuracies involved in the measurement of each of the scatter matrix elements and the usefulness of these measurements to the NEXRAD mission.

Hardware aspects that affect the measurement accuracies are isolation between the orthogonal channels and the phase and gain matching of the two channel receivers over the entire dynamic range. For example, the magnitude of the cross coupled power in the off-diagonal elements of the scatter matrix are calculated to be 20 to 35 dB below the power level in the main diagonal elements (Stapor and Pratt, 1984) depending on the rain rate. To measure these off-diagonal terms accurately the channel isolation has to be much better than 35 dB.

Channel isolation of greater than 35 dB is beyond the state of the art for certain of the microwave components needed in these systems. In particular the circulators required can presently deliver a guaranteed isolation of about 20 dB with typical isolation of about 22 dB and matched system isolation of less than 25 dB. In the proposed radar system designs the switchable circulators are the limiting component. Orthomode couplers and scalar feeds can deliver an isolation greater than 40 dB. With the present hardware, measurement of the off-diagonal components will require accurate characterization of the radar system so that the bias error produced by channel cross-coupling in the radar can be compensated for by computation.

There are no reported measurements of the complete scattering matrix so far, though the technical feasibility of designing a polarization agile radar has been reported (Schroth **et al.**, 1982, Metcalf **et al.**, 1980). Most of the reported dual polarization measurements are confined to Z_{DR} and CDR. Of these two parameters, Z_{DR} has been used more successfully to increase the accuracy of rainfall rate estimate.

2.2.1 Z_{DR} Measurement

Z_{DR} is defined as the ratio of horizontal reflectivity Z_H to vertical reflectivity Z_V, and is related to the scatter matrix [s] and drop size distribution (DSD) N(D) by

$$Z_{DR} = \frac{Z_H}{Z_V} = \frac{\int_0^{D_m} |S_{HH}|^2 \, N(D) \, dD}{\int_0^{D_m} |S_{VV}|^2 \, N(D) \, dD} \tag{2.6}$$

where integration is over all drop sizes from zero to the maximum drop size, D_m. It may be noted that Z_{DR} is a function of only the diagonal terms of the scatter matrix, hence there is no need to estimate the cross-coupled components.

Radar transmission is alternately switched between horizontal and vertical polarizations and only the co-polarized signal is received using a single receiver. This single receiver scheme eliminates the need for extremely good polarization discrimination in the orthomode coupler and dual receiver matching. Z_{DR} is computed from the received complex voltage samples E_H and E_V, usually by either the square law estimator or log ratio estimator. These Z_{DR} estimators are defined by Bringi, et al. (1983).

$$\hat{Z}_{DR} = \frac{<|E_H|^2>}{<|E_V|^2>} \quad \text{; square law estimator} \tag{2.7}$$

$$\hat{Z}_{DR} = <10 \log \left[\frac{|E_H|^2}{|E_V|^2}\right]> \quad \text{; log ratio estimator} \tag{2.8}$$

2.2.2 CDR Measurement

In CDR measurement the transmission is in either RHC or LHC polarization and both the co-polar and cross-polar circular components are received simultaneously. Measurements of two received components simultaneously require two matched receivers, and because the cross-coupled component is several orders of magnitude smaller (typically <-15 dB), the channel isolation also has to be very good. In practice it has been found that CDR of less than -25 dB cannot be measured very reliably (Nathanson, 1969). CDR is estimated as the expected value of the ratio of co-polar to cross-polar power returns, expressed in dB's.

If all the scatterers are oriented in a common direction, CDR is related to the scattering matrix [S] elements and drop size distribution by the relation

$$\mathrm{CDR} = \frac{\int_0^{D_m} |S_{HH} - S_{VV}|^2 \, N(D) \, dD}{\int_0^{D_m} |S_{HH} + S_{VV}|^2 \, N(D) \, dD} \tag{2.9}$$

It can be shown that the CDR is independent of mean canting angle and is a function of drop shape only.

2.2.3 Comparison of Z_{DR} and CDR Measurements

Ideally, Z_{DR} and CDR are related to each other via the scatter matrix elements and DSD. For a monodisperse DSD, Z_{DR} and CDR are related by the transformation

$$CDR = \left(\frac{1 - Z_{DR}^{1/2}}{1 + Z_{DR}^{1/2}}\right)^2 \qquad (2.10)$$

Comparison of equations (2.6) and (2.9) suggests that CDR may provide the same or more information than Z_{DR}, particularly since CDR depends on the mean shape of the scatters regardless of their orientation, while Z_{DR} depends on shape as well as orientation. However, CDR measurement imposes stringent performance requirements on the radar system in terms of channel isolation and receiver matching. More important, CDR is severely affected by propagation effects which limit its usefulness to situations where the propagation effect is small. While the requirement of receiver matching can be overcome by alternately measuring co-polar cross-polar components using the same receiver, the state of the art isolation achievable (~25 dB) is marginal and the propagation effect must be accounted for. McGuinness **et al.** (1984) present data and model predictions which imply that propagation effects through 10 km of uniform rain can be ignored if rainfall rate is less than 20 mm/h. For 40 mm/h a gate-by-gate correction is mandatory and for a rate of 80 mm/h correction is impossible.

Measurement of Z_{DR} is simpler than CDR measurement. Its effectiveness in the estimation of precipitation rate depends on the alignment of scatterers in horizontal and vertical directions, which is usually good in rain. However, the important advantage of Z_{DR} measurement is that it is not seriously affected by propagation.

If in addition to Z_{DR} one of the cross coupled components is also measured (which increases the complexity of the radar system), a canting angle can be estimated. Unfortunately this measured canting angle would not be the true mean canting angle of the hydrometeors in the resolution volume, but would be biased by the canting angle of the drops along the propagation path.

2.2.4 Differential Propagation Phase Shift Constant, $\Delta\phi$, Measurement

Differential phase shift constant $\Delta\phi$ is also a differential measure dependent on hydrometeor shape and orientation and $\Delta\phi$ in combination with Z_H can be used to calculate the two unknown parameters of DSD. It may be noted that the measurement of $\Delta\phi$ does not involve additional microwave hardware. It can be estimated from the same time series used for Z_{DR} estimation. Unlike Z_{DR}, $\Delta\phi$ is a parameter of the forward scatter matrix. It may prove to be useful in hydrometeor identification if both Z_{DR} and $\Delta\phi$ are computed, since the behavior of these two parameters in relation to Z_H may vary significantly for a given hydrometeor type. A combination of Z_H, Z_{DR} and $\Delta\phi$ may prove more useful than Z_H and Z_{DR}. An important use could be for hail discrimination in severe thunderstorms. It is well known that hailstones coated with water have backscatter cross sections similar to water drops of the same size but the differential propagation phase shift characteristics may be significantly different for water-coated hail and water drop of the same size.

While differential phase shift has been studied by communication engineers extensively in order to assess the depolarizing effect on communication channels (Morrison **et al.**, 1973 and 1973b; Oguchi and Hosaya, 1974; Fang and

Chen, 1982), there are no reported measurements of $\Delta\phi$ using meteorological radar, nor has it been used in determining rain rate. Seliga and Bringi (1978) address the possibility of using $\Delta\phi$ for the determination of DSD parameters in one of their early papers. Measurement aspects such as the accuracy to which $\Delta\phi$ can be estimated and the statistics of $\Delta\phi$ have to be investigated in order to evaluate the usefulness of $\Delta\phi$ in meteorological studies.

2.3. Possible Enhancement of NEXRAD Products

For meteorological radars the polarization properties of the scatterers provide information about the geometry and thermodynamic phase state of the scattering medium. This information, not available in measurements of Z and spectral moments, provides estimates of scattering parameters which normally are assumed. If this new information is sufficiently accurate the radar could provide better measurements of such weather features as:

Rainfall rate both at a point and over an area.

Location of the melting layer.

Identification of hydrometeor type most notably discrimination between hail, snow, rain, supercooled droplets, etc.

In the following sections we discuss how the Z_{DR} information can improve these measurements.

2.3.1 Rainfall Rate Measurement

Doppler radar with single polarized transmission measures the scattered power from the meteorological targets and estimates the equivalent reflectivity, Z, of the resolution volume. The reflectivity is related to the total water content of the resolution volume but accurate determination of water content and rain rate, R, from radar reflectivity requires knowledge of drop size distribution. The conventional method has been to use an empirical Z-R relationship such as $Z = aR^b$, where a and b are empirical constants (Battan, 1973). Several authors have determined these constants from the DSD measured with disdrometers. Through numerous measurements reported in the literature it has been established that a large variability in the DSD exists, and naturally occurring drop size distributions having the same Z have rainfall rates which differ by as much as a factor of 4 (Doviak & Zrnic, 1984).

Most notable among the proposed drop size distributions and probably the most widely used, is the two-parameter exponential distribution (Marshall and Palmer, 1948). Based on their measurements and those of Laws and Parsons (1943) Marshall and Palmer proposed that,

$$N(D) = N_0 e^{-\Lambda D} \tag{2.11}$$

$N_0 = 8 \times 10^3\ m^{-3}\ mm^{-1}$, $\Lambda = 4 \cdot 1\ R^{-0.21}\ (mm^{-1})$ where D is the drop diameter and R is the rain rate in mm/hr. Measurements of Joss **et al.** (1968) show that the two parameters N_0 and Λ vary considerably for different types of rain such as drizzle, widespread showers, thunderstorms, etc. Furthermore, Pasqualucci (1984) observed that in a convective storm the parameters vary considerably from the edge of the storm to main shaft depending on the vertical wind velocity. These variations in DSD result in errors in the empirically determined rainfall rates and direct measurements to account for these variations in DSD are not practical.

Assuming the form of the DSD to be M-P distribution as given in (2.11) the parameters N_0 and Λ can be determined by Z_{DR} and Z_H measurement (Seliga & Bringi, 1976), or CDR and reflectivity at circular polarization (McGuinness

et al., 1984). Because of its superior immunity to propagation effects we consider only the Z_{DR}, Z_H technique. Studies by Seliga **et al.** (1980, 1981), in which the rain rates derived from differential reflectivity measurements were compared to the measured rain rates using rain gauge data and disdrometer data, show that improvement in dispersion of rain rate measurement is possible with Z_{DR} as compared to the empirical Z-R method. Seliga **et al.** (1981) report good agreement between Z_{DR} derived rain rate and the rain rate measured by rain gauges. Furthermore, Cherry **et al.** (1984) have refined the DSD hypothesis by showing that the assumption of an exponential drop size distribution leads to a consistent over-estimate of rainfall rate. They demonstrated that a gamma distribution removes virtually all systematic bias in rainfall rate estimation and also reduces the dispersion from 34% using empirical Z-R to 14% for the Z_{DR}.

Thus the additional information in the Z_{DR} could improve the rain rate estimates by radar. However, to achieve good accuracy in the rainfall rate measurement Z_{DR} must be estimated to within a fraction of a dB because it is the parameter which determines which drop sizes contribute most to the rain rate. Examinations of the relationship between Z, Z_{DR}, and derived rate (Figure 2.2) shows that the sensitivity of rain rate measurement to variation in the Z_{DR} estimate increases at smaller Z_{DR} values. With a fixed reflectivity of 45 dBZ and a Z_{DR} between 1.9 and 2.1 dB the rain rate would vary from 23 to 27 mm/h which is about 8% of the mean.

In more realistic terms, for $\hat{Z}_H$ of 45 dBZ and an error of ±0.5 dB then a $\hat{Z}_{DR}$ error of ±0.1 dB will result in a rainfall rate error of 20%. These rather stringent accuracy requirements imply long dwell times for estimation.

2.3.2 Location of the Melting Layer

It has been observed that Z, Z_{DR} and CDR have relative peak values below the zero degree isotherm. Generally the order of peaks in the vertical profiles is as follows: highest is the reflectivity peak, about 100 m below is the peak of CDR and 100 m below the CDR peak is the peak of Z_{DR}. The Z_{DR} peak is narrowest and hence delineates very precisely a height where hydrometeors have 90% melted (Moninger **et al.**, 1984). This information together with the distance between reflectivity peak and Z_{DR} peak may provide information about the thermodynamic characteristics of the melting layer and its thickness.

2.3.3 Identification of hydrometeor type

Measurements of reflectivity depolarization and differential reflectivity can be used to infer the type of hydrometeors responsible for the scattering. Table 1 from Hall **et al.** (1980) shows qualitative relationships between Z and Z_{DR} for various hydrometeors. Quantitative relationships have not been well established yet. Low, medium, and high Z correspond roughly to 30, 40, and 50 dBZ. Z_{DR} measurements in rain typically vary between 0.5 and 4 dB whereas in hail Z_{DR} is near 0 or negative (Bringi, Seliga, and Aydin, 1984). The location of hail signature ($Z>55$ dBZ and $Z_{DR}<0.2$ dB) and the profile of Z, Z_{DR} below it could indicate the potential for hail damage on the surface. This new technique is just now being investigated by several research groups. Another practical use of Z-Z_{DR} patterns may be in locating large super-cooled raindrops which may be hazardous to aviation.

3. METHODS FOR FOR DUAL POLARIZATION MEASUREMENTS

Dual polarization capability has been implemented both in linear and circular polarized radar systems. The most commonly measured parameter using dual polarization radar is either Z_{DR} or CDR. The Z_{DR} measurement is more useful for rain rate measurement and has more potential benefit for NEXRAD.

No text or figure on this page.

TABLE 1. Expected characteristics of Z and Z_{DR} at 10-cm wavelength for various hydrometeor types (From Hall et al., 1980).

Hydrometeor Type	Z	Z_{DR}	Comments
Rain	High	High	Includes large oblate drops
Drizzle, cloud, fog, or super cool drops	Low	Low	Small spherical drops of water and/or small ice particles
Dry snow flakes	Medium-low	Medium-low	Large horizontally oriented low-density aggregates
Sleet/wet snow	High	High	Large oblate horizontally oriented particles
Wet graupel	High	Negative	Large conical vertically oriented particles
Wet hail	High	Low	Large particles: seldom spheres
Dry hail or other high-density ice particles	Medium	Low	

	Parameter	
Relative Scale	Z	Z_{DR}
low	30 dBZ	0.5 dB
medium	40 dBZ	2 dB
high	50 dBZ	4 dB

3.1 Statistical Considerations

Data acquisition time is a prime consideration in the NEXRAD system. To meet the overall mission the system is required to have a volume throughput time less than five minutes where the volume consists of a full 360° scan at about 15-20 elevation angles. This implies an antenna scan rate of 3 to 4 rpm and a dwell time of 55 to 42 milliseconds per 1° azimuthal increment. For a scan rate of 3 rpm, a PRT of 1 ms, and an antenna BW of 1°, the number of samples available per beam width is about 48.

All the measurements of Z_{DR} available in the literature have been made using the alternate transmission of horizontal and vertical polarized fields as described in Section 3.2, and practical experience is that the number of samples required to accurately estimate Z_{DR} is very large (256 pulses with log received NCAR radar) for such a scheme. To decide whether the existing proven Z_{DR} measurement scheme can be adapted to the NEXRAD system and provide useful information, we need to consider the accuracy with which Z_{DR} can be measured with the limited number of contiguous E_H, E_V sample pairs available and the sensitivity of the computed rain rate to errors in Z_{DR} and Z_H or Z_V.

3.1.1 Z_{DR} Accuracy Requirement

Significant potential benefit of Z_{DR} to NEXRAD would be to improve rain rate measurements. Single polarized radar measurements of rain rate using empirical Z-R relationships provide a good estimate of the mean but a wide variation between storms. For example, Brandes and Sirmans (1976) report a mean gauge to radar ratio of 1.05 for 14 storms with a dispersion of 30%. Seliga **et al.** (1980) report a gauge to radar ratio of 0.62 with dispersion of 19%. These variations are due to the microphysical and kinematic processes that affect the drop size distribution and drop-fall speeds.

Calibration of radar measurements using rain gauges with a density of 1000-2000 km^2/gauge can reduce the average error to 30% (Wilson & Brandes, 1979). In one of their comparative radar and rain gauge measurement studies Seliga **et al.** (1980) use the data from a network of rain gauges and simultaneous radar measurement of rain rate with the Z_{DR} technique. Estimated standard error in Z_{DR} was 0.28 dB. Data from 317 rain gauges spread over an area of 5000 mi^2 were used to compare the Z_{DR} derived rain rate to the rain rate measured by the gauges. Their results show that the Z_{DR} derived rate dispersion is comparable or smaller than rain rate dispersion obtained from the Z-R relationship calibrated by rain gauges. However, rain gauge measurements themselves are subject to inaccuracies. In addition to the sampling error, wind conditions can cause an under-catch estimated to be as much as 20-40% (Wilson & Brandes, 1979) in the 10-35 $m \cdot s^{-1}$ outflow region of thunderstorms. To achieve 5% standard error, a network density of 20 km^2/gauge with 1 hr averaging time is necessary (Weisner, 1970), a highly impractical configuration for the NEXRAD radar network.

Rain rate is a very sensitive function of Z_H and Z_{DR} requiring highly accurate estimates of these parameters for accurate rainfall estimates. An error analysis by Goldhirsh (1984) shows that the rms deviation in the rain rate is as much as 100% for an error of -0.2 dB in Z_{DR} and calibration error of 2 dB in Z_H. The rms deviation in rain rate is approximately 20% for an assumed zero error in Z_H and an error of 0.2 dB in Z_{DR}. To estimate rain rate with less than 20% error, Z_{DR} has to be estimated with an accuracy of at least 0.1 dB, assuming Z_H is accurate to within 0.5 dB.

The theoretical curves presented in Figure 2.2, which give the relationship between Z_{DR} and rainfall rate with N_o and Z_H as parameters, illustrate the sensitivity of rainfall rate to errors in Z_H and Z_{DR}. At a given Z_H an error of 0.2 dB in Z_{DR} results in about 40% error in rainfall rate, where as at a given Z_{DR} an error of 1 dB in Z_H translates to approximately 40% to 50% error in rainfall rate. With a 1 dB error in Z_H and a 0.2 dB error in Z_{DR}, the estimated rainfall rate will have a larger than 50% error.

In addition to random zero mean errors the Z_H and Z_{DR} estimates are subject to systematic bias errors. Whereas variance of Z_{DR} and Z_H can be reduced by averaging samples, bias errors can be removed only if a priori knowledge of the signal handling process is available. Some factors that introduce bias errors in Z_H and Z_{DR} are receiver calibration, depolarization due to differential propagation phase shift, attenuation in the propagation path, and mismatch between the antenna patterns for horizontally and vertically polarized transmissions.

Because Z_{DR} is a differential measure and usually the same receiver is used for both horizontally and vertically polarized signals, the receiver calibration does not affect the Z_{DR}. However, it can introduce bias error in Z_H and thus the calibration error should be considerably better than 1 dB. Depolarization and attenuation due to propagation through the rain medium affect both Z_{DR} and Z_H estimates and produce systematic bias errors. Antenna pattern mismatch introduces a bias in Z_{DR} which is difficult to remove. It is essential that the main beams be matched to avoid any serious bias error in Z_{DR}. Beam pattern matching in the sidelobe region is in general very difficult and sidelobe mismatch can cause false Z_{DR} values especially when the main beam illuminates weak scatterers near large reflectivity gradients such as at the edge of storms (Herzegh and Carbone, 1984). For typical weather radar antennas Z_{DR} will not be affected by sidelobes if the total power received by the main lobe is at least 15 dB larger than the power through sidelobes.

3.1.2 Estimation of Z_{DR} by Alternate Sampling of E_H and E_V

The only established Z_{DR} measurement technique uses a polarization switch to alternately sample the vertically and horizontally polarized signals E_V and E_H. Z_{DR} is estimated from these samples using one of the three estimators, square law, log ratio, or ratio estimator. A recent paper by Bringi **et al.**, (1983) discusses the statistical properties of the Z_{DR} signal and compares the three estimators. Their analysis assumes classical Gaussian statistics based on a "random walk" model to derive standard deviation σ_{DR} of Z_{DR} and concludes that for a given dwell time the standard deviation of the Z_{DR} estimate is lowest for the square law estimator. Since minimum dwell time is of prime importance in the NEXRAD application this is the only estimator we will examine here. The square law estimator of Z_{DR} is defined as (Bringi **et al.**, 1983)

$$\hat{Z}_{DR} = \frac{\frac{1}{M}\sum_{i=1}^{M} |E_H|_i^2}{\frac{1}{M}\sum_{i=1}^{M} |E_V|_i^2} = \frac{\hat{P}_H}{\hat{P}_V} \tag{3.1}$$

The standard deviation of $\hat{Z}_{DR}$ is a function of the correlation coefficient between E_H and E_V signals and the decorrelation time of the signal. From a study of time series records with pulse repetition time of 1.6 ms Bringi **et al.** (1983) report a median value of the average pulse-to-pulse cross correlation coefficient of 0.965 and the standard deviation of $\hat{Z}_{DR}$ from 40 pairs of independent samples, between 0.1 to 0.25 dB while the standard deviation of $\hat{Z}_H$ and $\hat{Z}_V$ is between 0.7 to 1.5 dB. The observed decorrelation time of E_H and E_V signal varies between 6 and 45 ms so that an integration time of approximately 0.5 seconds is necessary to obtain 0.2 dB standard deviation in the Z_{DR} estimate (Bringi **et al.**, 1978).

Bringi **et al.** (1983), in their analysis of Z_{DR} signal statistics assume that the sample pairs E_H and E_V are independent. However, in practice, the averaging is done with contiguous pairs of samples and one cannot ignore the correlation that exists between the samples. Zrnic' (1979) examined the effect of correlation between contiguous samples in the calculation of spectral moments of weather signals. These results, with some simplifying assumptions can be used to predict the behavior of the Z_{DR} measurement. The variance of Z_{DR} can be approximated by

$$\mathrm{var}(Z_{DR}) \hat{=} \frac{2\,\hat{Z}_{DR}^{\,2}}{M^2} \sum_{m=-(M-1)}^{(M-1)} (M - |m|)\,[|\rho(2m)|^2 - |\rho(2m+1)|^2\,|\rho_{HV}(0)|^2] \quad (3.2)$$

where M is the number of contiguous E_H or E_V samples, $\rho(m)$ is the correlation coefficient between E_H (or E_V) samples for m pulse lag and $\rho_{HV}(0)$ is the correlation coefficient between E_H and E_V samples for zero lag.

Normalizing (3.2) with respect to $(Z_{DR})^2$, fractional standard deviation, σ_{DR}, in dB's is

$$\sigma_{DR}(\mathrm{db}) = 10 \log \left(\frac{Z_{DR} + \sigma_{DR}}{Z_{DR}}\right) \mathrm{dB} \quad (3.3)$$

A similar analysis for variance of the Z_H estimate gives

$$\mathrm{var}(Z_H) = Z_H^2 \sum_{m=-(M-1)}^{(M-1)} \frac{(M-|m|)|}{m^2}\,\rho(2m)|^2 \quad (3.4)$$

Using (3.4) and (3.2) we can derive an inequality

$$\frac{var(Z_{DR})}{Z_{DR}^2} > 2\ (1-|\rho_{HV}(0)|^2)\ \frac{var(Z_H)}{Z_H^2} \tag{3.5}$$

From (3.3), (3.4) and (3.5) it follows that for a realistic value of $|\rho_{HV}(0)|^2 = 0.995$ the number of samples needed to keep the standard error of reflectivity below 0.5 dB is sufficient to keep also σ_{DR}(db) below 0.1.

The signal correlation function and spectral density constitute a Fourier transform pair. For a Gaussian spectral density $\rho(m)$ can be expressed as

$$|\rho(m)|^2 = e^{-4\pi^2 w^2 T_s{}^2 m^2} \tag{3.6}$$

where $wT_s = \sigma_v/2v_a$, σ_v is the standard deviation of velocity spread, v_a is the unambiguous velocity and T_s is the pulse repetition time. These correlation coefficients are signal properties which are not under our control. Spectral widths of weather echoes range from about 1 m s^{-1} for snow and stratiform rain to about 10 m s^{-1} in the mesocyclone. The median value for convective storms is about 4 m s^{-1}.

The relations between M and σ_{DR} plotted in Figures 3.1 to 3.4 show that σ_{DR} decreases with increasing spectrum width for a given M, but has a lower limit at $WT_s \approx 0.078$ corresponding to σ_v = 5 m s^{-1} (T_s = 1 ms). Even when the orthogonal signal correlation $|\rho_{HV}(0)| = 1.0$ (ideal case-see Figure 3.1) the value of σ_{DR} is 0.12 dB at M=25 (M compatible with NEXRAD specification) for σ_v = 4 m s^{-1}. For larger spectrum widths σ_{DR} is larger with Z_{DR} becoming unusable at σ_v = 6 m s^{-1}. It is shown in the Appendix that $|\rho_{HV}(0)|^2$ is generally larger than 0.995. Thus the values of σ_{DR} given in Figure 3.2 should represent practical values. This figure gives a value σ_{DR} = 0.17 dB for M = 25 and σ_v= 4 m s^{-1}. However, stronger turbulence (σ_v>4 m s^{-1}) is likely to induce oscillations of drops so that the pair correlation $\rho_{HV}(0)$

would decrease which in turn would tend to increase σ_{DR}. Thus, in order to maintain the required data throughput rate some additional variance reduction method must be used.

Spatial averaging is a means of reducing the reflectivity and differential reflectivity estimate variance. A continuous integration in range (Wallace, 1953) or averaging of discrete samples spaced close enough to approximate a continuous integration provides a variance reduction factor M_e (number of statistically independent samples); related to the number of pulse depths, m, that are averaged by

$$M_e = 3m/2 + 3/8 \tag{3.7}$$

In the NEXRAD some range averaging would perhaps be acceptable provided the Z and Z_{DR} scales of interest are greater than the 3 dB cutoff scale of the averaging process. The cutoff scale is 2.2 ΔR, where ΔR is the averaging length (Sirmans and Doviak, 1973). Some averaging of reflectivity is allowed to provide a range resolution compatible with the angular resolution of the 1° BW antenna. The radar sample volume width and height is approximately 1 km at a range of 60 km. Assuming a pulse width $\tau_s = 1.6$ µs, we obtain 6.4 independent samples by range averaging over 1 km. This range averaging over 1 km reduces the decibel standard error of Z_{DR} by a factor of 2.5. In dB's this corresponds to a standard deviation reduction from 0.17 dB to 0.07 dB at a σ_v of 4 m s^{-1} and from 0.24 dB to 0.1 dB at a σ_v of 1 m s^{-1} which satisfy the 0.1 dB criterion for σ_{DR}. To reduce σ_Z to 0.5 dB the range averaging interval for Z would have to be about 3.5 km.

3.1.3 Bias Error in Z_H and Z_{DR} Due to Propagation Through Rain

Raindrops are spheroidal in shape and tend to orient themselves with the small axis along the vertical. Thus the propagation constant is different for horizontally and vertically polarized waves. This difference in propagation causes depolarization and couples power into the orthogonally polarized field. It is shown in the Appendix that cross coupling is a function of both the two-way differential propagation phase shift, ϕ, and mean canting angle, θ. The cross coupling affects the measured E_H and E_V signals differently, in an alternate sampling scheme, resulting in bias errors in Z_H and Z_{DR} estimates. The bias errors, δZ_H, and δZ_{DR} due to propagation are given in Figures 3.5 and 3.6. These values are calculated at $Z_{DR} = 3$ dB. Figure 3.5 shows that Z_H is underestimated if $\theta > 0°$ and the error can be as much as -0.5 dB for $\phi = 180°$ and $\theta = 8°$. However, we do not expect the mean canting angle to be greater than 5° nor the differential phase shift greater than 180° even in severe storms. At 3 GHz a 50 mmh^{-1} rain over a propagation path length of 40 km is needed to produce a two-way differential phase shift of 180° (see Figure A.18). Under these conditions the bias errors in Z_H and Z_{DR} are within 0.2 dB and 0.1 dB respectively.

3.2 Acquisition Waveforms

If CDR is the parameter of interest it can be obtained from any acquisition scheme since each echo provides the LH and RH polarization powers simultaneously. Thus, Doppler spectral moment measurement and CDR measurement are waveform compatible although the acquisition times needed for accurate estimates will probably be quite different for the two parameters.

However, Doppler spectral moment and Z_{DR} are not waveform compatible. Mean velocity and width estimates made from alternate transmission of polarization (HVHVHV) as shown in Figure 3.7 would have an increased standard error due to the modulation produced by unequal amplitudes of echoes with different polarizations. In addition to an increased variance the width estimate would be systematically biased.

In its simplest form the amplitude modulation can be viewed as a periodic change in signal strength (from pulse to pulse) which is reflected in the frequency domain as an increase in a colored noise power (i.e. sidebands around mean Doppler shift). The signal to noise degradation depends on the relative magnitude of the change (Z_{DR}). This decrease in equivalent signal to noise ratio results in an increase of standard errors in spectral moment estimates.

Even worse the mean autocovariance from such a scheme would be

$$\overline{R}(T) = |R(T)| \, e^{j\omega_d T} \cdot \cos\phi \tag{3.8}$$

where ϕ is the total differential phase shift between the two components, ω_d is the Doppler shift, and T is the sampling interval. The term $\cos\phi$ causes an ambiguity in the phase of the autocovariance whenever ϕ is outside a -90° to +90° interval. Furthermore, when ϕ is near 90° the errors in Doppler spectral moment estimates would be large because the cosine term in (3.8) attenuates the autocovariance. It is very difficult to account for the cumulative contribution of the propagation path to this shift.

The scheme shown in Figure 3.8a splits the samples available in the dwell time in equal number of pairs for $\hat{V}$ and $\hat{Z}_{DR}$ estimations. Estimates are extended to two range intervals by knowing the range distribution of echoes and use of multilag storage as implied in Figure 3.8b. The number of pairs for spectral moment estimation is reduced to one-half of available from a fixed polarization which results in an increase in the estimate variance of about a factor of $\sqrt{2}$. The increase in variance of $\hat{V}$ and $\hat{W}$ would be greater than $\sqrt{2}$ at low signal to noise ratios (<10 dB) since there is not a common sample in the formation of the pairs. The 24 alternate sample pairs for Z_{DR} estimation result in an estimate standard deviation of about 0.18 to 0.26 dB which could be perhaps reduced to about 0.1 dB with a range integration of 1 km. Determining the true range distribution of the echoes will have a significant impact on system throughput rate. If a batch waveform is used, the number of samples available for velocity and Z_{DR} measurement is reduced by about 2 and resulting estimate standard deviation is increased by about 20%.

In summary, compared to the present NEXRAD methods this scheme in conjunction with an unambiguous range distribution waveform would provide spectral moment estimate over two ambiguous range intervals with modification of data handling, but the mean velocity and width estimate standard deviation would be greater than 1.2 m s^{-1} instead of 1 m s^{-1}. In addition, even with a range averaging of 1 km the standard deviation of the differential reflectivity would be greater than the 0.1 dB required for improving the rainfall rate estimate over the empirical Z-R technique.

Other schemes can be devised which improve some aspect of the estimation at the expense of other aspects. For example, the scheme shown in Figure 3.8c would improve the estimate of Z_{DR} at the expense of the spectral moments by providing 36 sample pairs for Z_{DR} estimation and 12 sample pairs for spectral moment estimation with a 48 sample dwell. The estimate standard deviations would be about 1.4 m s^{-1} for velocity and width and 0.1 dB for Z_{DR} with range averaging of 1 km. Note that no allowance is made for an interlaced low PRF for unambiguous measurement of range.

3.3 Acquisition Time

The volume acquisition time of the NEXRAD is dictated by the meteorology. The five to six minutes allowed for acquisition of the data is about the maximum time interval which will meet the forecasting and monitoring mission of the system. Base data accuracies are constrained by this acquisition time, the radar system characteristics and data spacial resolution. The system is presently specified at close to its maximum capability, i.e., minimum variance estimation schemes are used; the standard deviation of the estimates are about as large as tolerable for reliable product generation; close to maximum spatial averaging is done and the system provides the data at the required throughput but with little or no excess time. Incorporation of the requirement for a signal measurement incompatible with the base data measurement will obviously involve a significant change in the system acquisition scheme and its ability to address the prescribed mission.

There are two general ways to approach this problem. One is to add the hardware necessary to make the new measurement and modify the operational methods so as to accommodate both types of measurements which will involve compromising some aspect of the existing system capability. Another is to impose the new requirement of Z_{DR} estimation in addition to all existing requirements. This would require a redesign of the RDA.

3.3.1 Modified Operational Scheme

Two alternatives in operational schemes and the resulting impact on the system capability which may be considered are:

- Reduction in antenna rotation rate by a factor of two and increased averaging in range to 3 km.

The increased number of samples provided by this would allow the existing accuracy in spectral moment estimates to be maintained and provide the Z_{DR} measurement with the accuracy required. However, the throughput time would be 10 minutes (about twice that of the present NEXRAD Technical Requirement), (NTR), probably too large for adequate severe weather forecasting and certainly too large for use at aviation terminals. A range integration increment of 3 km results in a cut off scale of about 6 km. This may limit the utility of the Z_{DR} measurement in features like the gust front, hail shaft, mesocyclone, etc., which have dimensions of this order.

- Measurement of Z_{DR} only during one scan at a slow rotation rate ($4° s^{-1}$) and low elevation angle.

The greater number of samples provided by the slow rotation rate in conjunction with some range averaging allows measurement of Z_{DR} with the required accuracy. However, the 1 1/2 minutes required for the scan adds directly to the overall throughput time. More serious is the question of usefulness of a Z_{DR} measurement at only one elevation angle. Probably the only utility would be for rainfall measurement and locating hydrometeor type near ground.

3.3.2 Engineering Redesign

Absorption of the Z_{DR} measurement in addition to the existing spectral moment measurement will require a more efficient technique for measuring both Z_{DR} and spectral moments. Theoretically the simultaneous measurement of horizontally and vertically polarized return power has the potential for increasing the throughput rate of the Z_{DR} measurement. However, the technique is unproven and untested and will require substantial engineering development, and, if implemented on NEXRAD, would require a redesign of the RDA. This technique is examined in detail in the Appendix. Basically, the scheme consists of simultaneous transmission and reception of both horizontally and vertically polarized signals. Simultaneous measurement of the horizontally and vertically polarized return powers has the obvious advantage of decreasing the time required to acquire a given number of samples which shortens the data throughput time for a prescribed accuracy. However, to deliver a suitable measurement, methods must be derived to handle the problems associated with the propagation of the two polarizations such as attenuation and differential phase shift as well as the hardware problems associated with dual signal processing such as orthogonal signal discrimination and receiver matching. These and other questions are examined in the Appendix. Preliminary calculations (Section 3.4.3) indicate that with careful design the simultaneous system sampling can deliver an estimate of both differential reflectivity and the spectral moments with the required accuracy and throughput rate if averaging of Z_{DR} over about 1 km in range and Z_H over a range interval of about 3 km is acceptable.

3.4. Microwave hardware

The microwave hardware unique to a dual linear polarization system is the antenna primary feed and microwave switching arrangement for delivering the two different polarizations. Unique signal processing consists of a multiplexer for the received signal and the Z_{DR} or CDR calculator. If full control over the switching is exercised such as with the latching ferrite circulators any desired polarization sequence can be implemented.

3.4.1 Measurement of Z_{DR}

A simplified block diagram (Figure 3.9) shows the components that would need to be added on a NEXRAD. Feed horn must be circular (or a scalar type) so that either field can be radiated. An orthogonal mode coupler would be inserted behind the feed to accept either vertical or horizontal fields. An additional waveguide would be installed from the orthomode coupler to the switch. The switch most likely would be situated behind the reflector along with associated power supplies. The signals to control the switch would be brought above the antenna rotation planes through slip rings. Signal processing for Z_{DR} estimation is done after the common receiver. The multiplexer behind the receiver is controlled by the transmitted sequence so that echoes from different polarizations are appropriately processed to obtain power estimates for horizontal and vertical polarizations. To reduce statistical uncertainty the samples are averaged in both time and range (see Sec. 3.1.2). The Z_{DR} estimate would be from either ratios of power or differences of logarithms of powers, depending on the algorithm chosen.

Although modifications are straightforward and the cost is modest compared to total radar system cost, there is some engineering risk and limitations on system measurement imposed by the hardware.

The significant engineering risks are in the microwave hardware design and fabrication. There is no significant risk in the signal processing hardware. To perform well, the dual polarized system will require a close match of the vertical and horizontal antenna secondary pattern. This in turn requires a close match of the primary feed pattern as well as the blockage characteristics of the reflector and feed support apparatus. However, the antenna criteria present only a small risk (but no small expense) since they represent stringent engineering design rather than new technology development. There is a significant risk in the design and development of the switchable ferrite circulator. Most circulators in use to date are not rated for the high peak and average power (1 MW, 1.5 kW) required of NEXRAD. While the production costs of the higher power units would probably be a small increase over the lower power units presently in service, the one-time engineering development cost would probably be about $500K. Another characteristic of the ferrite switch, which is more of a system limitation than an engineering risk, is the orthogonal isolation. The present technology can deliver a guaranteed isolation of about 20 dB with typical isolation of about 22 dB. It is not likely that this will improve with the existing materials and manufacturing techniques [ESI, 1983]. An isolation of 20 dB is adequate for the Z_{DR} measurements (diagonal elements of the scattering matrix) but marginal for full matrix measurements (diagonal and off diagonal elements).

3.4.2 Measurement of CDR

Referring to Figure 3.10 the hardware needed for CDR measurements consists of antenna feed horn and a microwave circulator to resolve the returned elliptical polarization into its LH and RH circular components. An additional receiver is needed for the orthogonal component and a signal processor for CDR calculation. CDR estimation imposes a more stringent antenna design criteria than linear dual polarization. However, it is possible by careful design of the antenna coupler to achieve good isolation with acceptable cross coupling. The incremental cost of implementing the circular depolarization ratio measurement is about the same as that of differential reflectivity. Note that CDR measurement is not from sequential signals but sample pairs of powers are obtained from each returned echo. Consequently the standard error of CDR estimates would be smaller, and unlike the Z_{DR} technique CDR measurements, do not affect the Doppler spectral moments. However, the susceptibility of this measurement to the propagation effects makes it an unattractive candidate for operational implementation.

3.4.3 Simultaneous Measurement of Z_{DR}

A block diagram of the simultaneous system is given in Figure 3.11. The transmitter signal is divided in half and applied to the horizontal and vertical ports of the orthomode coupler via transmit and receiver circulators in both channels and a switchable 0 or 180° phase shifter in the vertical channel. The antenna feed is oriented conventionally and horizontal and vertical modes are excited either in phase to produce a polarization phase rotated by +45°, or 180° out of phase to produce a polarization plane rotation of -45°. The received signal is decomposed into its horizontal and vertical components by the orthomode coupler and applied to the receiver switch via the T/R circulators. The receiver outputs are applied to the signal processor.

Switching the signal polarization between +45° and -45° allows advantage to be taken of the symmetry of the bias error in Z_H and Z_{DR} due to drop canting and differential phase shift. Since these errors are approximately zero mean odd functions of the canting angle $\delta_{H,DR}(\theta) = -\delta Z_{H,DR}(-\theta)$ switching the polarization plane by 90° is equivalent to switching θ which results in a cancellation of the bias when estimates are obtained from successive samples.

The return signal is also switched between two receivers at one half the transmitter rate. Switching receivers provides inherent compensation of small receiver mismatch errors and relaxes the matching required to a reasonable value for an acceptable bias. Switching at half the transmitter rate prevents the receiver mismatch from contaminating the spectral moment estimation on pulse pairs.

An example of the theoretical $\hat{Z}_{DR}$ estimate accuracy achievable with this scheme is given in Figure 3.12. It is seen that when square of the orthogonal signal correlation is 0.995, spectrum width is 4 m s^{-1} and dwell time is 50 ms (50 samples), the standard deviation of $\hat{Z}_{DR}$ for simultaneous sampling is 0.12 dB; about one half that for alternate sampling. This could be reduced to the 0.1 dB needed to improve the rainfall rate estimate over the empirical Z-R method, by range averaging.

Spectral moment estimation can be done on either horizontal or vertical signals or both. Moment estimation from spaced pairs rather than contiguous pairs containing a common pulse will result in negligible degradation at SNR > 10 dB. At lower SNR the NTR required performance may not be achievable.

The developmental engineering risk of this system is in the phase shifter and antenna feed. The shifter is high risk for 1° accuracy over the NEXRAD operational frequency and temperature range. This component would probably be frequency specified and environmentally controlled. Compared to the existing NEXRAD modified for alternate sampling, this scheme has the following differences.

Implemented as shown in Figure 3.11 the simultaneous system would have signal detection capability 3 dB below an alternate system for a given transmitter power and all other parameters equal.

The simultaneous system would have some capability of increasing the data acquisition rate for a specified accuracy by using both polarizations for spectral moment estimation and by increasing range averaging interval for the Z_H and Z_{DR} estimates.

3.5 Signal Processing Hardware

Estimation of differential reflectivity (or differential return power in practice) can be done in a variety of ways. With the three basic receiver response types (square law, linear, or logarithmic) and two techniques of ensemble averaging (average of ratios and ratio of averages) one can derive six algorithms for $\hat{Z}_{DR}$. However, as noted in Section 3.1 the most efficient algorithm in terms of minimum standard deviation for a given dwell time is the square law estimator (Bringi **et al.**, 1983). Acquisition time is of course a prime consideration in the NEXRAD system.

The proposed algorithm for $\hat{Z}_{DR}$ calculation is a straightforward implementation of equation (3.1) with addition of the logarithmic operation, i.e.,

$$10 \log \hat{Z}_{DR} = 10 \log \frac{\frac{1}{m} \sum_{n=1}^{m} |E_H|_n^2}{\frac{1}{m} \sum_{n=1}^{m} |E_V|_n^2} = 10 \log \frac{\hat{P}_H}{\hat{P}_V} \tag{3.8}$$

In the case of NEXRAD, $|E|^2$ can be derived from either the complex video samples, I, Q (output of linear receiver), or the logarithm of echo power, log P, (output of the log receiver) by

$$|E|_n^2 = I_n^2 + Q_n^2 \quad \text{or} \quad |E|_n^2 = \text{antilog } (\log P_n) \tag{3.9}$$

These operations require about the same amount of integrated circuits and hence are of equal cost. Averaging is done separately for each polarization with the estimate being the ratio of averages. The processor hardware characteristics are tabulated (Table 2) in the same fashion as other signal processors in the system (Sirmans, 1980).

It is seen that the hardware requirement and computational complexity is slightly greater than for the intensity integrator and less than for the velocity and width calculation.

Estimation of CDR involves essentially the same hardware consideration.

3.6. Summary

In general the information about the radar cross section of the scatterers, provided by measurements at orthogonal polarizations Z_{DR}, has the potential for improving the capability of the NEXRAD network radar. In particular this information could improve the rainfall rate estimate over that of an empirical reflectivity rainfall rate relationship and it could also aid in distinguishing the type of scatterer (i.e., ice or liquid water).

CDR measurements are of limited utility and questionable benefit for the NEXRAD. Propagation effects will limit the usefulness of this measurement to regions or storm systems with low rainfall rates where the composite effect is less than that corresponding to propagation through 10 km at rainfall rate of 80 mm/hr. Since these are not the regions of prime interest to the radar meteorologist the measurement would probably find little application in the network radar product generation.

Differential reflectivity has some potential for improving NEXRAD rainfall rate estimates and discrimination of the scatter phase. The state of the art engineering can provide the microwave hardware necessary for the basic measurement without new engineering development. Full scattering matrix measurement; i.e., estimation of the off diagonal as well as the diagonal parameters, is marginal with existing hardware but full matrix measurement would not be necessary to realize the prime benefits of the technique.

Implementation of the orthogonal polarization measurement on a radar committed fundamentally to measurement of the spectral moments will require substantial changes in either operational methods in conjunction with basic engineering changes or a redesign of a the RDA. The most restrictive aspect

TABLE 2

Differential Reflectivity Calculator

Algorithm	Square Law Z_{DR} Estimator
Input word length	12 bits
Number of range locations	1024
Storage word length	32 bits
Total memory	70K bits
Throughput rate	1 MHz
Output word length	8 bits
Computations	2 multiplications
	1 division
	2 summations (256 samples)
	1 add
	1 logarithmic operation (PROM)

of Z_{DR} measurement with the network radar is the signal transmission sequence and data acquisition time required. The transmission of alternate orthogonal polarizations required for estimation of Z_{DR} results in a degradation of spectral moments estimates with this pulse train and modification of the transmission sequence is necessary to accommodate both type measurements. This in itself results in a longer total dwell time for a given statistical accuracy of the estimates since the sequence cannot be optimized for either. The inherently longer dwell time for the Z_{DR} estimation causes a significantly longer acquisition time for the composite measurement. For example, if Z_H is accurate to within 0.5 dB with a mean of 45 dBZ, the Z_{DR} estimate needs to be accurate to 0.1 dB to provide a rainfall estimate error less than 20%. For the NEXRAD parameters the dwell time with alternate polarization required for Z_{DR} accuracy of 0.1 dB is about three times that required for spectral moments estimate accuracy of 1 m s^{-1}. Since these two types of measurements have incompatible waveforms the total acquisition time is almost the sum of the two times.

Thus, if a straightforward implementation of Z_{DR} on the NEXRAD is made (with equal range resolution of spectral moments and Z_{DR}) the antenna rotation rate would have to be decreased (increase in dwell time) by about a factor of four. This would increase the volumetric throughput time from about five minutes to about twenty minutes.

A combination of increased dwell time and range averaging could also be used to achieve the required accuracies. Reducing antenna rotation rate by two and range averaging of Z_{DR} over 3 km would provide a volumetric throughput of about 10 minutes and a Z_{DR} measurement on scales greater than 6 km.

If the Z_{DR} measurement at only a limited number of elevations (i.e. lower one or two) is sufficient these could be acquired at a slow rotation rate (about one fourth that of the operational rate). However, the scan time for Z_{DR} of about 1 1/2 minutes adds directly to the volumetric throughput time.

Theoretically, the method of simultaneous measurement of powers from horizontally and vertically polarized echoes could provide the required statistics with a dwell time of about twice that in the present NTR for equal range resolution of Z_{DR} and spectral moments. The simultaneous technique in conjunction with a 3 km range averaging of Z_H and Z_{DR} could in theory provide the estimates with the accuracy needed at the required throughput rate. However, this technique is unproven and would require extensive engineering development and testing before acceptance. If accepted, the technique would require a major redesign of the present NEXRAD transmitter to maintain the present detection capability in addition to the receiver and antenna subsystems modification necessary for the Z_{DR} measurement.

LIST OF FIGURES

Fig. 3.7 Alternate transmission sequence. Correlations of interest are indicated.

Fig. 3.8 Possible transmission sequences for NEXRAD.

Fig. 3.9 Block diagram of the dual linear polarized radar for Z_{DR} measurement by alternate sampling of E_H and E_V signals.

Fig. 3.10 Block diagram of the circular polarized radar for CDR measurement.

Fig. 3.11 Block diagram of radar system for Z_{DR} measurement by simultaneous sampling of E_H and E_V.

Fig. 3.12 Standard deviations of differential reflectivity, σ_{DR}, with simultaneous and alternate sampling.

REFERENCES

Battan, L.J., 1973: Radar Observation of the Atmosphere. University of Chicago Press, Chicago, IL.

Beard, K.V., D.B. Johnson, and A.R. Jameson, 1983: Collisional forcing of raindrop oscillations. J. Atmos. Sci., 40, pp. 455-462.

Brandes, E.A., and D. Sirmans, 1976: Convective rainfall estimation by radar: Experimental results and proposed operational analysis technique. Preprints, Conference on Hydro-meteorology (Ft. Worth), AMS, Boston, MA, pp. 54-59.

Bringi, V.N., S.M. Cherry, M.P.M. Hall, and T.A. Seliga, 1978: A new accuracy in determining rainfall rates and attenuation due to rain by means of dual polarization radar measurements. IEEE International Conf. on Antennas and Propagation.

Bringi, V.N., T.A. Seliga, and S.M. Cherry, 1983: Statistical properties of the dual-polarization differential reflectivity (Z_{DR}) radar signal. IEEE Trans. Geosci. and Remote Sensing, Vol. GE-21, p. 215-220.

Bringi, V.N., T.A. Seliga, and K. Aydin, 1984: Hail detection with differential reflectivity radar. Science, Vol. 225, pp. 1145-1147.

Bringi, V.N., J. Vivekanandan, J.D. Tuttle, T.A. Seliga, and K.. Aydin, 1984: Joint analysis of dual-wavelength and dual-polarization (Z_{DR}) radar measurements during Maypole. Preprints, 22nd Conference on Radar Meteorology, Zurich, Switzerland, pp. 415-420.

Carbone, R.E., R.J. Serafin, and C. Frush, 1982: CP-2 Radar Developments. Preprints, URSI Symp. on Multiple Parameter Radar Measurements of Precipitation, Bournemouth, U.K., p. 70-72.

Cherry, S.M., and J.W.F. Goddard, 1982: The design features of dual-polarization radar which affect the accuracy of measuring differential reflectivity. Preprints, URSI Symp. on Multiple-Parameter Radar Measurements of Precipitation, Bournemouth, U.K., pp. 49-54.

Cherry, S.M., J.W.F. Goddard, and M. Ouldridge, 1984: Simultaneous measurements of rain by airborne disdrometer and dual-polarization radar. Radio Sci., 19, p. 169-176.

Doviak, R.J., and D.S. Zrnic', 1984: Doppler Radar and Weather Observations. Academic Press, (Ch. 8, P. 1).

Electromagnetic Sciences, Inc., 1983: Technical Bulletin #030475-4, #0200182-3, #031579-1. 125 Technology Park, Atlanta, GA 30092.

Fang, D.J., and C.H. Chen, 1982: Propagation of centimeter/millimeter waves along a slant path through precipitation. Radio Sci., 17, p. 989-1005.

Goddard, J.W.F., and S.M. Cherry, 1984: Quantitative precipitation measurements with dual linear polarisation radar. Preprints, 22nd Conference on Radar Meteorology, Zurich, Switzerland, , pp. 352-357.

Goldhirsh, J., 1984: An error analysis of the two polarization radar methods for determining rain rate using drop size spectra measured at Wallops Island, Virginia. Report No. S1R84U-014, John Hopkins University, Applied Physics Laboratory.

Green, A.W., 1975: An approximation for the shapes of large rain drops. J. Appl. Meteor., 14, pp. 1578-1583.

Hall, M.P.M., S.M. Cherry, J.W.F. Goddard, and G.R. Kennedy, 1980: Raindrop sizes and rainfall rate measured by dual polarization radar. Nature, Vol. 285, pp. 195-198.

Hendry, A., and Y.M.M. Antar, 1984: Precipitation particle identification with centimeter wavelength dual-polarization radars. Radio Sci., 19, pp. 115-122.

Herzegh, P.H., and R.E. Carbone, 1984: The influence of antenna illumination function characteristics on differential reflectivity measurements. Preprints, 22nd Conference on Radar Meteorology, Zurich, Switzerland, pp. 281-286.

Humphries, R.G., 1974: Depolarization effects at 3 GHz due to precipitation. Stormy Weather Group Report MW-82, McGill University.

Joss, J., J.C. Thams, and A. Waldvogel, 1968: The variation of raindrop size distributions at Locarno. Proceedings, Int. Conf. on Cloud Physics, Toronto, Ontario, Canada, p. 369-373.

Laws, J.O., and D.A. Parsons, 1943: The relation of raindrop size to intensity. Trans. Amer. Geophys. Union, 24, p. 452-460.

Marshall, J.S., and W. McK. Palmer, 1948: The distribution of rain drops with size. J. of Meteor., 5, p. 165-166.

McCormick, G.C., 1975: Propagation through a precipitation medium: Theory and measurement. IEEE Trans. on Antennas and Propagation, Vol. AP-23, pp. 266-269.

McCormick, G.C., and A. Hendry, 1975: Principles for the radar determination of the polarization properties of precipitation. Radio Sci., 10, p. 421-434.

McGuinness, R., A.R. Holt, and R.G. Humphries, 1984: The interpretation of CDR radar dta to obtain rain rates in storms. Preprints, 22nd Conference on Radar Meteorology, Zurich, Switzerland, pp. 276-280.

Metcalf, J.I., et al., 1980: Design study for a coherent polarization diversity radar. AFGL-TR-80-0262, Air Force Geophys. Lab.

Moninger, W.R., V.N. Bringi, T.R. Detman, J.R. Jordan, T.A. Seliga, and K. Aydin, 1984: Melting layer Observations during Maypole. Preprints, 22nd Conf. Radar Meteor., Zurich, Switzerland, pp. 364-369.

Morrison, J.A., and T.S. Chu, 1973: Perturbation calculations of rain induced differential attenuation and differential phase shift at microwave frequencies. Bell. Syst. Tech. Jl., 52, p. 1907-1913.

Morrison, J.A., M.J. Cross, and T.S. Chu, 1973: Rain drop induced differential attenuation and differential phase shift at microwave frequencies. Bell. Syst. Tech. Jl., 52, p. 599-604.

Nathanson, F.E., 1969: Radar Design Principles. McGraw-Hill Book Co., New York, N.Y.

Oguchi, T., 1977: Scattering properties of Pruppacher-Pitter form raindrops and cross polarization due to rain: Calculations at 11, 13, 19.3 and 36.8 GHz. Radio Sci., 12, pp. 41-51.

Oguchi, T., 1983: Electromagnetic wave propagation and scattering in rain and other hydrometeors. Proceedings IEEE, pp. 1029-1078.

Oguchi, T. and Y. Hosaya, 1974: Scattering properties of oblate rain drops and cross polarization of radio waves due to rain (Part II): Calculations at microwave and millimeter wave regions. J. Radio Res. Labs. (Japan), 21, p. 191-259.

Pasqualucci, F., 1984: Drop size distribution measurements in convective storms with a vertically pointing 35-GHz Doppler radar. Radio Sci., 19, p. 177-184.

Schroth, A., P. Meischner, and H. Schuster, 1982: Technical concept of the planned agile coherent polarization diversity radar for the DFVLR. Preprints, URSI Symp. on Multiple Parameter Radar Measurements of Precipitation, Bournemouth, U.K., p. 67-69.

Seliga, T.A., K. Aydin, and V.N. Bringi, 1984: Differential reflectivity and circular depolarization ratio radar signals and related drop oscillation and propagation effects in rainfall. Radio Sci., 19, p. 81-89.

Seliga, T.A., and V.N. Bringi, 1976: Potential use of radar differential reflectivity measurements at orthogonal polarizations for measuring precipitation. J. Appl. Meteor., 15, p. 69-76.

Seliga, T.A., and V.N. Bringi, 1978: Differential reflectivity and differential phase shift: Applications in radar meteorology. Radio Sci., 13, p. 271-275.

Seliga, T.A., V.N. Bringi, and H.H. Al-Khatib, 1981: A preliminary study of comparative measurements of rainfall rate using the differential reflectivity radar technique and a rain gauge network. J. Appl. Meteor., 26, pp. 1362-1368.

Seliga, T.A., V.N. Bringi, and E.A. Mueller, 1980: Comparison of rainfall rates derived from differential reflectivity and disdrometer measurements. Preprints, 19th AMS Conf. on Radar Meteor., Amer. Meteor. Soc., Boston, p. 523-525.

Sirmans, D., 1980: NEXRAD radar subsystem evolution study. Internal Report to JSPO, July 1980.

Sirmans, D., and R.J. Doviak, 1973: Meteorological radar signal intensity estimation. NOAA Tech. Memo. ERL-NSSL-64, Norman, OK, 80 pp.

Stapor, D.P., and T. Pratt, 1984: A generalized analysis of dual-polarization radar measurements of rain. Radio Sci., 19, pp. 90-98.

Ulbrich, C.W., and D. Atlas, 1984: Assessment of the contribution of differential polarization to improved rainfall measurements. Radio Sci., 19, p. 49-57.

Wallace, P.R., 1953: Interpretation of the fluctuating echo from randomly distributed scatterers, Part II. Canadian Journal of Physics, 31, pp. 995-1009.

Weisner, C.J., 1970: Hydrometeorology. Chapman and Hall Ltd., London, p. 232.

Wilson, J.W., and E.A. Brandes, 1979: Radar measurement of rainfall - a summary. Bull. Amer. Meteor. Soc., 60, p. 1048-1058.

Zrnic', D.S., 1979: Estimation of spectral moments for weather echoes. IEEE Trans. on Geosci. Electronics, Vol. GE-17, No. 4, p. 113-1-128.

APPENDIX

Simultaneous Dual Polarization Measurements

A.1. Z_{DR} Measurement Criteria Compatible With NEXRAD Specifications

From the statistical considerations of Z_{DR} signal as discussed in Chapter 3, we can conclude that Z_{DR} has to be estimated within 0.1 dB accuracy to be useful for better rain rate computation. It was also shown that to obtain less than 0.1 dB standard deviation of Z_{DR}, the averaging time or the number of samples required is large and cannot be obtained with the scan rate specified for NEXRAD. A scan rate of $18° s^{-1}$ precludes more than about 50 samples per estimate if azimuthal smearing is to be less than 50% of the beam width. Therefore, in order to make the Z_{DR} measurement compatible with NEXRAD we need to devise ways of estimating Z_{DR} within 0.1 dB using less than 50 contiguous samples (pulses). If alternate sampling scheme is used only 25 sample pairs are available per Z_{DR} estimate.

Alternate sampling scheme (Figure 3.9) is shown to be not very practical in terms of simultaneous measurement of spectral moments (see Sec. 3.2). Any other sampling sequence (e.g., see Figure 3.8) further increases the variance of Z_{DR} estimate.

In order to arrive at a measurement scheme compatible with NEXRAD specifications, it is not only necessary to devise means of reducing σ_{DR} but also of retaining the capability to estimate the spectral moments simultaneously with Z_{DR} measurement. One of the schemes that may have such a capability is simultaneous sampling of E_H and E_V signals as suggested in Section (3.3). This scheme provides vertically and horizontally polarized samples for every pulse transmission, thus retaining the spectral moments estimation capability. Further it also gives us as many sample pairs as the number of transmitted pulses, thus reducing the σ_{DR} in a given time, as compared to alternate sampling scheme which provides only half the numbers of sample pairs.

An analysis of the variance of Z_{DR} estimate using simultaneous sampling of E_H and E_V shows that the functional form of var(Z_{DR}) is similar to that for var(Z_H) but has an additional multiplying factor. Var(Z_{DR}) can be approximately expressed as

$$\mathrm{var}(Z_{DR}) = 2Z_{DR}^{2}\,(1-|\rho_{HV}(0)|^{2}) \sum_{m=-(M-1)}^{(M-1)} (M-|m|)\,|\rho(m)|^{2} \qquad \text{(A.1)}$$

The same notations are used as in Section 3. Plot of σ_{DR} expressed in dB's (see Eq. 3.5) versus the number of sample pairs M is presented in Figs. A.1 to A.3 for $|\rho_{HV}(0)|^2$ = 0.995, 0.99 and 0.98 respectively, with spectrum width as a parameter. σ_{DR}= 0.0 for $|\rho_{HV}(0)|^2$ = 1.0, is the ideal case of perfect correlation. For pair correlation better than 0.995, σ_{DR} spans 0.2 to 0.1 dB for spectrum widths between 1 and 4 ms^{-1} for M=50. It is shown later in this section that pair correlation better than 0.995 can be expected in practice. However, for narrow spectrum widths (<1 ms^{-1}) σ_{DR} is more than 0.2 dB and σ_Z is greater than 1 dB (given by Eq. 3.6). This standard error can be reduced to less than 0.1 dB by spatial averaging over 6 to 9 range samples.

There are several problems associated with simultaneous sampling. Important among these are propagation effect, receiver mismatch and cross polar discrimination which introduce bias errors in Z_H and Z_{DR} estimates. In order to assess the range of values that can be expected for pair correlation $|\rho_{HV}(0)|^2$, we consider several factors that decorrelate E_H and E_V signals. Bias errors and their compensation is considered later in this appendix.

A.1.1 Non-Spherical Drop Shape and Drop Oscillations

The resolution volume consists of a large number of scatterers of different shapes and sizes depending on their thermodynamic phase state. We consider only raindrop scatterers in this study. Raindrops are known to take up oblate spheroidal shapes and the oblateness or (b/a-axis ratio) is a function of drop size. For a given equivolumetric diameter D_e of the drop, the equilibrium axis ratio b/a, is given by Green's equation (Green, 1975). Figure A.4 shows the variation of a/b ratio with equivolumetric diameter for this equilibrium model (solid curve a in the figure). Because the distribution of drop shapes follows their size distribution the vector sum of the horizontally polarized scattered fields and the vector sum of vertically polarized fields are slightly decorrelated. Further, the drops can oscillate between oblate and prolate spheroidal shapes about a mean a/b ratio. These oscillations are generally induced by drop collision and break up and can be assumed to have random phases, hence the measured Z_{DR} is proportional to time averaged mean a/b rather than the equilibrium a/b. Beard **et al.** (1983) have shown that this mean is slightly higher than equilibrium a/b (see Figure 4 curve b). The oscillation amplitudes are dependent on collision energy and its decay rate. For the purpose of computing the decorrelation due to the drop shape and oscillation we assume a truncated Gaussian distribution of drop shapes about the oscillation mean a/b as given by Beard **et al.** (1983). The standard deviation of a/b about the mean is taken to be 1/3 maximum amplitude which is also the truncation point of the distribution (Figure A.5). The standard deviation and maximum and minimum truncation values of a/b are a function of equivolumetric diameter D_e (Figure A.4). The form of variation of these limits are approximated from the observed maximum and minimum values of a/b (Figure A.4, curve c), as reported in the literature. Drop size distribution $N(D)$ is assumed to be exponential Marshall-Palmer type ($N(D_e) = N_0 e^{-\Lambda D_e}$) with $N_0 = 8{,}000$. The raindrops are assumed to be at a temperature 0°C and the corresponding refractive index value of $m = \sqrt{\varepsilon_r} = 8.99 + j\,1.475$ at 3 GHz was used in the computation.

The computed theoretical values for the correlation coefficient $\rho_{HV}(0)$ due to drop shape and oscillation are presented in Figure A.6. With oscillating drops it can be noted that $|\rho_{HV}(0)|^2$ is better than 0.99 for rain rates less than 200 mmh^{-1}. Correlation is > 0.995 when the drops are not oscillating.

A.1.2 Canting Angle Distribution

In the analysis of decorrelation due to drop shape and oscillations, it was assumed that all the drops are oriented along vertical-horizontal direction. However, in nature, drops can have other orientations due to shear and turbulence in the resolution volume. Oguchi (1977) has constructed a raindrop distribution model with randomly canted drops for propagation studies. One of the important assumptions he made is that the canting angle is statistically independent of drop size. The canting angle distribution is assumed to be Gaussian with a mean θ_0 and standard deviation σ_θ. The mean θ_0 introduces a bias error in the measured Z_{DR} but does not contribute to decorrelation of E_H, E_V signals. The correlation coefficient $|\rho_{HV}(0)|^2$ is a function of σ_θ but is independent of θ_0. In order to get an idea of the upper limit of the decorrelation due to canting angle distribution, we consider a mono-disperse drop size distribution with $D_e = 5$ mm. Five to 8 mm is the maximum diameter of the drops observed in rain with bigger drops in higher rain rates. We also assume Gaussian distribution for the canting angles with zero mean and standard deviation σ_θ. The canting angle distribution is given by

$$N(\theta) = \frac{1}{\sqrt{2\pi}\,\sigma_\theta}\, e^{\frac{-\theta^2}{2\sigma_\theta^2}} \qquad (A.2)$$

An equilibrium shape with a/b = 0.68 corresponding to a 5 mm drop D_e is used in the computation. The correlation coefficient $|\rho_{HV}(0)|^2$ for mono-disperse DSD is given in Figure A.6. This figure shows that $|\rho_{HV}(0)|^2$ is better than 0.995 required for compatibility with NEXRAD even for very large standard deviation of $\sigma_\theta = 18^0$. For the rain with exponential DSD the correlation is better than this number because the smaller the drop is, the less is the eccentricity of the drop, reducing the effect of canting on $|\rho_{HV}(0)|^2$.

A.1.3 Decorrelation due to antenna scanning

Antenna scanning shifts the resolution volume from pulse to pulse. Any gradient in the Z_{DR} will be averaged to produce a mean value. Even when there is no gradient and the rain field is uniform, scanning reduces the signal decorrelation time, and hence $\rho_{HV}(1)$ for alternate sampling. An approximate relation for computing the correlation coefficient is given by Doviak and Zrnic' (1984).

$$\rho_{HV}(1) = e^{-2\ln(2)/n^2} \qquad (A.3)$$

where n is the number of samples (or transmitted pulses) in the time it takes to scan the one-way (-3dB) beam width of the antenna. For NEXRAD scan rate of 18° s^{-1}, 1° BW and 1 ms PRT, this correlation coefficient is better than 0.999. For simultaneous sampling the scanning would not affect the pair correlation. The decorrelation due to antenna scanning is very small even for alternate sampling, and hence it can be neglected.

A.1.4 Decorrelation Due to Doppler Velocity Spread

Doppler velocity spread is mainly responsible for signal decorrelation with time, but does not affect $|\rho_{HV}(0)|^2$ because of zero time lag. For a Gaussian spectra the correlation coefficient is given by (3.8). The variation of $|\rho(1)|^2$ for one pulse lag with spectrum width is given in Figure A.6.

All these considerations establish that the only possible way of making Z_{DR} estimation compatible with NEXRAD specifications is to sample E_H and E_V simultaneously. We propose a scheme of measurement in the next section and consider the possible accuracy of Z_{DR} measurement, and advantages and disadvantages of the scheme.

A.2. Z_{DR} Measurement With Simultaneous Sampling

A schematic of the proposed simultaneous E_H, E_V sampling system is given in Figure A.7. To sample E_H and E_V simultaneously, pulse transmission at 45° linear polarization is used. The horizontally polarized and vertically polarized waveguide modes are excited in phase in the antenna feed to rotate the polarization plane by exactly 45°. A power divider channels equal power into E_H and E_V ports of the orthomode coupler. In the receiving mode the two circulators channel the horizontally and vertically polarized signals into two separate phase and gain matched receivers. A phase shifter, switchable between two phase settings of 0° and 180°, is introduced in the transmission path of the vertically polarized signal so that the polarization plane can be switched between +45° and -45° with respect to horizontal. This switching is incorporated to compensate for the propagation effect which is explained later in this section.

While simultaneous sampling makes it possible to obtain highly correlated sample pairs (E_H, E_V), we encounter additional problems due to propagation and hardware. There are three important aspects, namely the propagation effect, polarization discrimination in the antenna coupler and receiver mismatch, which must be investigated for the order of error these factors introduce in the measurement of Z_H, Z_{DR}, mean Doppler velocity, etc. These factors do not affect the variance of Z_{DR} but introduce a bias error in the Z_{DR} and Z_H measurement. We consider each factor separately and suggest methods to compensate for these errors. It is shown that with the implementation of the suggested bias error compensation, Z_{DR} estimation within 0.1 dB accuracy is possible except in the most severe cases of propagation contamination.

A.2.1 Propagation Effect

The transmitted pulse propagates to the resolution volume and back through the intervening precipitation medium. Because of the preferred orientation of the scatterers in the propagation medium, the attenuation and phase shift for the horizontally and vertically polarized waves differ. Together the differential propagation properties and the canting angle of the hydrometeors in the propagation path cause a cross coupling between vertically and horizontally polarized propagating fields, leading to bias error in the measured Z_{DR} and Z_H. It is extremely difficult to evaluate the propagation effect exactly for a complex precipitation medium of varying reflectivities, canting angle and phase state, along the propagation path. However, the order of error can be evaluated using simplified models such as a uniform rain field.

In order to understand the propagation effect on Z_H, Z_{DR} measurements we consider the theory of propagation through rain medium briefly. Propagation of electric field E through rain is governed by the differential equation

$$\frac{dE}{dz} = ME \tag{A.4}$$

where z is the path length in the propagation direction and the column matrix $E = \begin{bmatrix} E_H \\ E_V \end{bmatrix}$. The 2 x 2 matrix M is the sum of two matrices M_o and M_I. M_o is the free space propagation matrix given by

$$M_o = \begin{bmatrix} -jk_o & 0 \\ 0 & -jk_o \end{bmatrix} \tag{A.5}$$

where k_o is the propagation constant for the free space. The matrix M_I is a product of three matrices and is given by

$$M_I = \begin{bmatrix} \cos\theta & -\sin\theta \\ \sin\theta & \cos\theta \end{bmatrix} \begin{bmatrix} f_{11} & f_{12} \\ f_{21} & f_{22} \end{bmatrix} \begin{bmatrix} \cos\theta & \sin\theta \\ -\sin\theta & \cos\theta \end{bmatrix} \tag{A.6}$$

θ is the canting angle of the scatterers in the elemental path length δz and the matrix [f] is the forward scatter matrix for this elemental path length. The off-diagonal terms f_{12} and f_{21} are zero if all the scatterers have the same canting angle θ, and are negligible if canting angle has symmetric distribution about mean θ. In general, the elements of [f] depend on the canting angle distribution as well as drop size distribution.

The solution of the simultaneous differential equation (A.4) is obtained in terms of the eigenvalues and eigenvectors of the matrix M and can be expressed as (Oguchi, 1983)

$$[E_r] = [T]\,[E_t] \tag{A.7}$$

where [T] is known as the transmission matrix. The subscript t and r represent transmitted and received fields. The elements of [T] are functions of mean canting angle θ and differential phase shift ϕ.

The solution (A.7) is for uniform rain field of propagation path length z. In general, the rain field is not uniform - the rain rate, drop size distribution, mean canting angle, etc., vary along the propagation path which makes the solution of equation (A.4) very difficult. However, an approximate solution can be obtained by dividing the propagation path into several uniform rain field subsections and cascading the solution as proposed by McCormick (1975).

To evaluate the effect of propagation on reflectivity and differential reflectivity measurements, we consider a uniform rain medium with rain rate and mean canting angle constant along the entire propagation path z. Given the horizontally and vertically polarized transmitted field, E_H^t and E_V^t, the received field components E_H^r and E_V^r will contain cross-coupled terms if the mean canting angle differs from zero. Cross coupling is a function of mean canting angle and the differential propagation phase shift ϕ.

The analysis presented so far is for one-way propagation. In the case of a radar the forward propagation from the radar to the resolution volume and the reverse propagation from resolution volume to the radar antenna have transmission matrices whose off-diagonal terms have opposite signs due to the change in propagation direction. Since we are evaluating the effect of propagation only, for simplicity, we assume that the canting angle of the drops in the resolution volume is zero and hence the scatter matrix [S] for the resolution volume has only diagonal terms. The received fields can then be expressed as

$$\begin{bmatrix} E_H{}^r \\ E_V{}^r \end{bmatrix} = \begin{bmatrix} T_{11} & T_{12} \\ T_{21} & T_{22} \end{bmatrix} \begin{bmatrix} S_{11} & 0 \\ 0 & S_{22} \end{bmatrix} \begin{bmatrix} T_{11} & T_{12} \\ T_{21} & T_{22} \end{bmatrix} \begin{bmatrix} E_H{}^t \\ E_V{}^t \end{bmatrix} \qquad (A.8)$$

For simultaneous E_H, E_V sampling scheme (Figure A.7) the transmitted fields $E_H{}^t$ and $E_V{}^t$ are equal. From the scatter matrix for the resolution volume, the true Z_H and Z_{DR} can be expressed as

$$\left.\begin{aligned} Z_H &= \langle|S_{11}|^2\rangle \\ &\text{and} \\ Z_{DR} &= \frac{\langle|S_{11}|^2\rangle}{\langle|S_{22}|^2\rangle} \end{aligned}\right\} \qquad (A.9)$$

Putting $E_H{}^t = E_V{}^t = 1.0$ in (A.8), we can evaluate the measured reflectivity X_H and measured differential reflectivity X_{DR} using square law estimators:

$$\left.\begin{aligned} \hat{X}_H &= \langle|E_H{}^r|^2\rangle \\ &\text{and} \\ \hat{X}_{DR} &= \frac{\langle|E_H{}^r|^2\rangle}{\langle|E_V{}^r|^2\rangle} \end{aligned}\right\} \qquad (A.10)$$

At S-band frequencies (3 GHz) the path attenuation is very small (Fang and Chen, 1982), so we consider only the differential phase shift. The total differential phase shift ϕ is a function of path length z and rain rate via drop size distribution.

From (A.8) and (A.10) the estimated values of X_H and X_{DR} can be expressed in terms of the elements of the transmission matrix and the true values of Z_H and Z_{DR} as,

$$\begin{aligned}\hat{X}_H &= <|E_H^r|^2> = <|S_{11}|^2>|A|^2 + <|S_{22}|^2>|B|^2 + <S_{11}S_{22}^*> AB^* + <S_{11}^*S_{22}> A^*B \\ &= Z_H|A|^2 + Z_V|B|^2 + <S_{11}S_{22}^*> AB^* + <S_{11}^*S_{22}> A^*B\end{aligned} \tag{A.11}$$

$$\hat{X}_V = <|E_V{}^r|^2> = Z_H|C|^2 + Z_V|D|^2 + <S_{11}S_{22}^*> CD^* + <S_{11}^*S_{22}> C^*D \tag{A.12}$$

and

$$\hat{X}_{DR} = \frac{\hat{X}_H}{\hat{X}_V} = \frac{Z_{DR}|A|^2 + |B|^2 + Z_{DR}^{1/2}\ (AB^* + A^*B)}{Z_{DR}|C|^2 + |D|^2 + Z_{DR}^{1/2}\ (CD^* + C^*D)} \tag{A.13}$$

where
$$\begin{aligned}A &= (T_{11}{}^2 + T_{11}T_{12}) \\ B &= (T_{12}T_{22} + T_{12}{}^2) \\ C &= (T_{12}T_{11} + T_{12}{}^2) \\ D &= (T_{22}{}^2 + T_{12}T_{22})\end{aligned}$$

The transmission matrix elements are path-integrated values and therefore can be assumed to be constant over the sampling interval. From equations (A.9), (A.11) and (A.13) the bias error in the estimated values of Z_H and Z_{DR} can be expressed as

$$\delta Z_H = \left(\frac{\hat{X}_H - Z_H}{Z_H}\right)100\ \%;\ \text{or}\ \delta Z_H = 10\log\left(\frac{\hat{X}_H}{Z_H}\right)\ \text{dB.} \tag{A.14}$$

and $$\delta Z_{DR} = \left(\frac{\hat{X}_{DR} - Z_{DR}}{Z_{DR}}\right)100\ \% \text{ or } \delta Z_{DR} = 10 \log\left(\frac{\hat{X}_{DR}}{Z_{DR}}\right) \text{ dB.} \qquad (A.15)$$

Equation (A.13) shows that the bias error in the estimated Z_H and Z_{DR} values is a function of mean canting angle (contained in the T matrix), differential propagation phase shift and the true Z_{DR} of the resolution volume. The error can be significant for large propagation phase shifts. For a propagation phase shift of 90° and true Z_{DR} = 3 dB the error in $\hat{X}_{DR}$ can be as much as 50% for a mean canting angle $\theta = 8^0$. In general, canting angle in a rain medium is distributed about zero mean. The effect of canting angle distribution is to reduce the differential propagation constant thus reducing the propagation effect (Oguchi, 1983). Further, differential phase shift per kilometer is small at 3 GHz and it would take a propagation path length of at least 40 km in 50 mmh^{-1} rain to produce a two-way differential phase shift of 180°. The error due to two way differential propagation phase shift ϕ increases as ϕ increases from 0° to 90° and then the error decreases to zero when $\phi = 180^0$. For ϕ beyond 180° the error increases rapidly and can be more than 50% at $\phi = 360^0$. Though these kinds of phase shifts are uncommon in nature, it is desirable to compensate for this bias error to increase the usefulness of Z_{DR} measurement.

It was observed in the course of bias error computation that the functional form of the bias error with ϕ is similar for mean canting angles $+\theta$ and $-\theta$ (θ measured from horizontal) with a change in sign. An error compensation scheme was devised based on this fact. Referring to Figure A.7, the polarization of the transmitted pulse is switched alternately between +45° and -45° to the horizontal by changing the phase of the vertical input by 180°. This is equivalent to switching canting angles between $+\theta$ and $-\theta$, as far as the bias error in Z_{DR} and Z_H is concerned. X_{DR} and X_H are estimated using expressions (A.10) except that the successive samples are obtained from +45° and -45° polarized transmissions.

The bias error δZ_{DR} for +45° transmissions for various canting angles is presented in Figure A.8 as a function of two-way differential phase shift. The true Z_{DR} of the resolution volume is +3dB and the error is expressed in decibels. It can be seen that the two sets of curves for $+\theta°$ and $-\theta°$ transmission are nearly symmetric about the zero line. However, the error cancellation is not perfect because of a small asymmetry between the two sets of curves. The bias error, when alternate switching of polarization planes is employed, is a monotonically increasing function of ϕ, but the error is drastically reduced from that of +45° transmission alone (Figure A.9). Figures A.10 through A.14 give the error for different Z_{DR} values, positive as well as negative.

Corresponding bias error in Z_H for a 45° polarization and alternate polarization switched scheme are given in Figures A.15 and A.16. These show that the error cancellation is more effective in Z_H than in Z_{DR}. After compensation error in Z_H is less than 0.26 dB for ϕ = 360° and θ = 10° which is better than that for alternate sampling (Figure 3.7).

To get an idea of the order of differential phase shifts encountered in nature we present the theoretically computed values of the two-way differential propagation phase shift ϕ per kilometer path length versus rain rate, at 3 GHz transmission frequency. The values in Figure A.17 are computed using an exponential drop size distribution ($N(D)=N_o e^{-\Lambda D}$; $N_o=0.8 \times 10^4\ m^{-3} mm^{-1}$). Figure A.18 presents the differential phase shift versus propagation path length for various rain rates. Uniform rain rate over the entire path length has been assumed in the computation.

A.2.2 Polarization Discrimination in the Antenna Coupler

The dual polarization capability Doppler radar antenna uses a scalar feed horn with an orthogonal mode transducer to separate the vertically and horizontally polarized received signals. Though these two modes are theoretically orthogonal, there are practical limitations in separating the powers in these two polarizations due to the cross coupling between the two ports. The entire assembly of horn feed and the orthomode transducer can be characterized using a scatter matrix [a]. If E_H and E_V are the horizontally and vertically polarized incident fields on the antenna and V_A and V_B are the outputs of horizontal and vertical channels respectively, then the V_A and V_B can be expressed in terms of E_H, E_V as,

$$\begin{bmatrix} V_A \\ V_B \end{bmatrix} = \begin{bmatrix} a_{11} & a_{12} \\ a_{21} & a_{22} \end{bmatrix} \begin{bmatrix} E_H \\ E_V \end{bmatrix} \tag{A.16}$$

where matrix [a] is the scatter matrix of the feed and coupler. Although the complete scatter matrix is a 4 x 4 matrix for the four port network, we consider only part of the matrix (i.e. E_H, E_V inputs and V_A, V_B outputs) corresponding to the power flow in the receive mode. The elements $a_{11} = a_{22} = 1.0$ and $a_{12} = a_{21}^* = \alpha$ is the cross coupling (symmetric coupler). There is a lower limit to the achievable cross coupling factor and the residual cross-coupled power introduces a bias error in Z_{DR} estimate.

To evaluate this error we set Z_{DR} estimated using E_H, E_V as the true Z_{DR} and the one estimated using V_A, V_B as the measured differential reflectivity X_{DR}.

$$\hat{Z}_{DR} = \frac{\langle |E_H|^2 \rangle}{\langle |E_V|^2 \rangle} \tag{A.17a}$$

$$\hat{X}_{DR} = \frac{<|V_A|^2>}{<|V_B|^2>} \tag{A.17b}$$

Using (A.16) $\hat{X}_{DR}$ and $\hat{Z}_{DR}$ can be related via equation,

$$\hat{X}_{DR} = \frac{\hat{Z}_{DR} + |\alpha|^2 + \hat{Z}_{DR}^{1/2}\, 2\mathrm{Re}(\alpha^* \rho)}{1 + |\alpha|^2\, \hat{Z}_{DR} + \hat{Z}_{DR}^{1/2}\, 2\mathrm{Re}(\alpha^* \rho)} \tag{A.18}$$

where Re(•) indicates real part and ρ is the correlation coefficient between E_H and E_V samples.

For simultaneous sampling of E_H and E_V, it has been shown in the previous section that the correlation coefficient $|\rho|^2$ is better than 0.995. However, because of the differential propagation phase shift and the differential reflection phase shift at the scatterer (this is very small - less than 0.2° and hence can be neglected) the phase of ρ is an unknown parameter. The scatter matrix of the coupler can be exactly determined by measurements.

Taking the inverse of the coupler scatter matrix [a] and using the definitions in (A.17), we can express the true Z_{DR} in terms of the measured value $\hat{X}_{DR}$. Taking the inverse of matrix [a],

$$[a]^{-1} = \frac{1}{1 - |\alpha|^2} \begin{bmatrix} 1 & -\alpha \\ -\alpha^* & 1 \end{bmatrix} \tag{A.19}$$

and using (A.17a) we have,

$$\hat{Z}_{DR} = \frac{\hat{X}_{DR} + |\alpha|^2 - \hat{X}_{DR}^{1/2}\, 2\mathrm{Re}(\alpha^* \rho_v)}{1 + \hat{X}_{DR}\, |\alpha|^2 - \hat{X}_{DR}^{1/2}\, 2\mathrm{Re}(\alpha \rho_v)} \qquad \text{(A.20)}$$

In (A.20) the correlation coefficient ρ_v is between V_A and V_B which can be estimated along with $\hat{X}_{DR}$. If α is determined accurately, the error in Z_{DR} can be corrected using (A.20).

It is desirable to reduce α to a lowest possible value by fine tuning the coupler, and further improvement in Z_{DR} estimate can be made using (A.20). It may be noted here that a coupling factor $|\alpha|^2$ less than -35 dB leads to an error level of less than 0.1 dB in Z_{DR} without the correction factor applied. Because radar operates at a fixed frequency and the frequency can be made extremely stable, it should be possible in practice to fine tune the ortho-mode coupler for less than -35 dB cross coupling.

A.2.3 Bias Error Due to Receiver Mismatch

For accurate measurement of Z_{DR} the two receivers (see Figure A.7) have to be matched in gain. Phase matching is needed if the differential phase shift between E_H and E_V samples is being measured. Because meteorological signals have large dynamic range (>80 dB), perfect phase and gain matching of the receivers over the entire dynamic range is very difficult. Power gain has to be matched to within 0.1 dB (approximately 2.5 %) accuracy to maintain Z_{DR} bias error less than 0.1 dB. Suggested here is a scheme which reduces the bias error in Z_{DR} due to receiver mismatch. It is shown that with this scheme a 10% mismatch in the gains of two receivers translates to less than 0.1% bias error in the estimated Z_{DR}.

A schematic of the hardware is shown in Figures A.19 and A.20. The received signals E_H and E_V are switched between the receivers R_1 and R_2

alternately with each pulse transmission. A second switch S_2, in synchronism with S_1, switches the outputs to the proper horizontal and vertical channels so that the subsequent circuits need not be altered.

Let the power gain of receiver R_1 be $G_1 = G$ and that of R_2 be $G_2 = G+\delta G$. If E_{Hi} and E_{Vi} are the horizontal and vertical signal inputs, the corresponding outputs V_{Hi} and V_{Vi} can be written as,

$$\begin{aligned} V_{Hi} &= E_{Hi} G_1^{1/2}\,;\ i = 1, 3, 5, \ldots \\ V_{Hi} &= E_{Hi} G_2^{1/2}\,;\ i = 2, 4, 6, \ldots \\ V_{Vi} &= E_{Vi} G_2^{1/2}\,;\ i = 1, 3, 5, \ldots \\ V_{Vi} &= E_{Vi} G_1^{1/2}\,;\ i = 2, 4, 6, \ldots \end{aligned} \tag{A.21}$$

The estimated horizontal and vertical reflectivities are proportional to

$$\hat{Z}_H = \langle V_H\ V_H^* \rangle = \frac{G}{M} P_{H1} + \frac{2\delta G}{M} P_{H2} \tag{A.22}$$

and

$$\hat{Z}_V = \langle V_V\ V_V^* \rangle = \frac{G}{M} P_{V1} + \frac{2\delta G}{M} P_{V2} \tag{A.23}$$

where $P_{H1} = \sum_{i=1}^{M} |E_{Hi}|^2$; $P_{H2} = \sum_{i=1}^{M/2} |E_{H2i}|^2$; $P_{V1} = \sum_{i=1}^{M} |E_{Vi}|^2$ and $P_{V2} = \sum_{i=1}^{M/2} |E_{V(2i-1)}|^2$.

The true value of the differential reflectivity at the input of the receiver is

$$\hat{Z}_{DR} = \frac{P_{H1}}{P_{V1}} \tag{A.24}$$

Denoting the estimated value of differential reflectivity as $\hat{X}_{DR}$,

$$\hat{X}_{DR} = \frac{\langle |V_H|^2 \rangle}{\langle |V_V|^2 \rangle} = \frac{\hat{Z}_{DR} + \dfrac{2\delta G \, P_{H2}}{G \, P_{V1}}}{1 + \dfrac{2\delta G \, P_{V2}}{G \, P_{V1}}} \tag{A.25}$$

For sufficiently large M the ratio of summations in the numerator and denominator of (A.25) tend to $\hat{Z}_{DR}$ and unity respectively, making $\hat{X}_{DR} = \hat{Z}_{DR}$, i.e., zero bias error.

For some finite M we can write:

$$\frac{2P_{H2}}{P_{V1}} = \hat{Z}_{DR}\,(1+a)$$

and

$$\frac{2P_{V2}}{P_{V1}} = (1+b)$$

where a and b are fractional errors ($|a|$, $|b| \ll 1$) which tend to zero for large M. The measured value $\hat{X}_{DR}$ remains accurate when $|\rho_{HV}(0)|^2 \approx 1{\cdot}0$ because the fractional errors a and b are equal. If the correlation coefficient is less than unity, the fractional errors are different in general. This gives rise to some residual error in $\hat{X}_{DR}$ given by

$$\hat{X}_{DR} = \hat{Z}_{DR} \left[\frac{1 + \frac{\delta G}{G}(1+a)}{1 + \frac{\delta G}{G}(1+b)} \right] \tag{A.26}$$

For a 10% error in receiver gain match (i.e., $\frac{\delta G}{G} = 0.1$) and 10% difference in a and b ($\rho \approx 0 \cdot 9$), the error in measured differential reflectivity $\hat{X}_{DR}$ is approximately 0.1%.

In this analysis of receiver switching we have assumed that the input sequence E_H and E_V is ideal. In the simultaneous measurement of E_H and E_V as suggested in this report (Figure A.[illegible]) the successive samples are obtained using +45° and -45° transmission to compensate for the propagation effect. When polarization switching and receiver switching are used simultaneously it can lead to errors in the measured Z_{DR}. To avoid this the receiver switching rate has to be half that of polarization switching. The receivers are switched once in two pulse transmissions. This procedure also removes the bias error in the mean velocity due to phase mismatch in receivers, when pulse pair processing is used.

FIGURE CAPTIONS

Fig. A.1 Standard deviation, σ_{DR}, versus number of pairs, M, for simultaneous sampling of E_H and E_V, $|\rho_{HV}(0)|^2 = 0.995$.

Fig. A.2 Standard deviation, σ_{DR}, versus M for simultaneous sampling of E_H and E_V, $|\rho_{HV}(0)|^2 = 0.99$.

Fig. A.3 Standard deviation, σ_{DR}, versus M for simultaneous sampling of E_H and E_V, $|\rho_{HV}(0)|^2 = 0.98$.

Fig. A.4 Axis ratio a/b versus equivolumetric drop diameter D_e. (a) Equilibrium shape, (b) time averaged a/b for oscillating drops, (c) upper and lower limits of a/b for oscillating drops.

Fig. A.5 Truncated Gaussian distribution of a/b ratios.

Fig. A.6 Pair correlation coefficient variation with rainfall rate R for oscillation model; standard deviation σ_θ of canting angle distribution; variation of $|\rho(1)|^2$ with spectrum width.

Fig. A.7 Block diagram of radar for simultaneous sampling of E_H and E_V.

Fig. A.8 Bias error δZ_{DR} variation with two way differential propagation phase shift ϕ for transmission at +45° polarization and simultaneous sampling of E_H and E_V. Mean canting angle θ is shown as a parameter. True value of Z_{DR} is 3 dB.

Fig. A.9 Bias error δZ_{DR} after compensation. Transmission is switched between ±45° polarizations alternately; Z_{DR} = 3dB.

Fig. A.10 δZ_{DR} versus ϕ after compensation; Z_{DR} = 2 dB.

Fig. A.11 δZ_{DR} versus ϕ after compensation; Z_{DR} = 1 dB.

Fig. A.12 δZ_{DR} versus ϕ after compensation; Z_{DR} = -1 dB.

Fig. A.13 δZ_{DR} versus ϕ after compensation; Z_{DR} = -2 dB.

Fig. A.14 δZ_{DR} versus ϕ after compensation; Z_{DR} = -3 dB.

Fig. A.15 Bias error δZ_H versus two way propagation phase shift ϕ with θ as a parameter for +45° polarized transmission; Z_{DR} = 3 dB.

Fig. A.16 Bias error δZ_H versus ϕ after compensation; ±45° polarized transmission; Z_{DR} = 3 dB.

Fig. A.17 Two way differential phase shift per km versus rainfall rate R.

Fig. A.18 Two way differential phase shift ϕ versus path length z with R as a parameter.

Fig. A.19 Schematic of receiver switching for mismatch compensation.

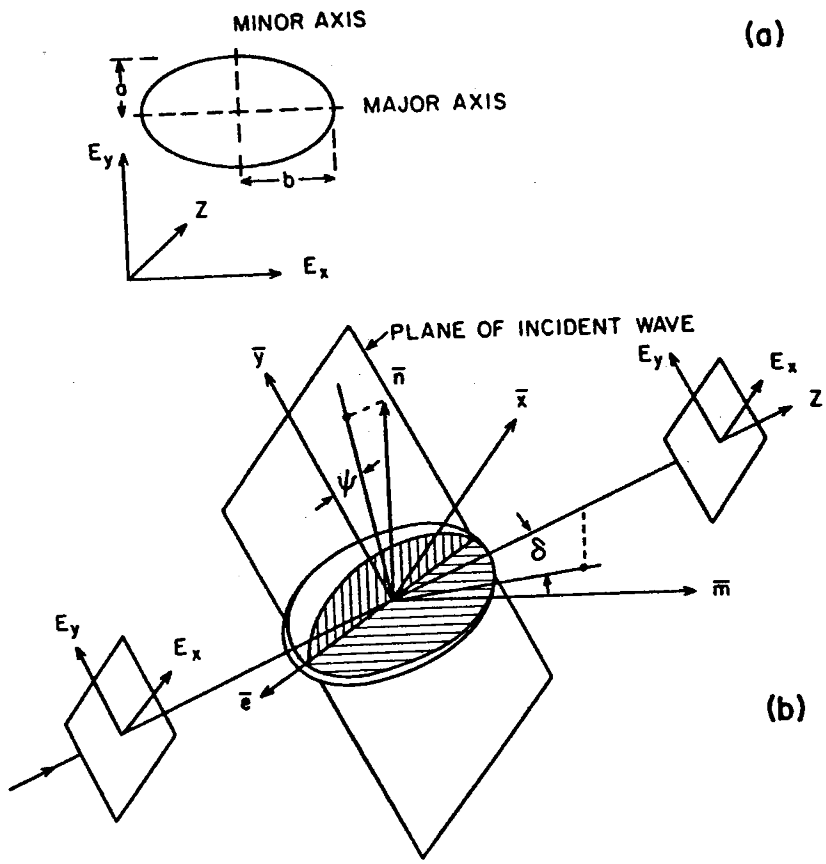

Fig. 2.1 The geometry of raindrop scattering.

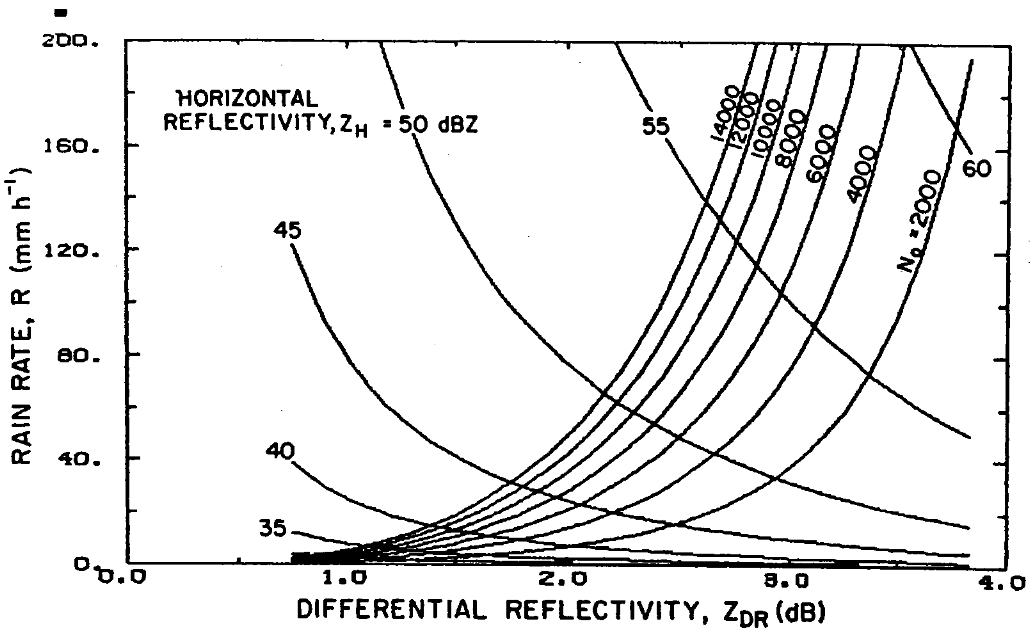

Fig. 2.2 Relation between differential reflectivity, Z_{DR}, and rainfall rate, R, for exponential DSD. The Marshall-Palmer distribution corresponds to $N_0 = 8000\ m^{-3}mm^{-1}$.

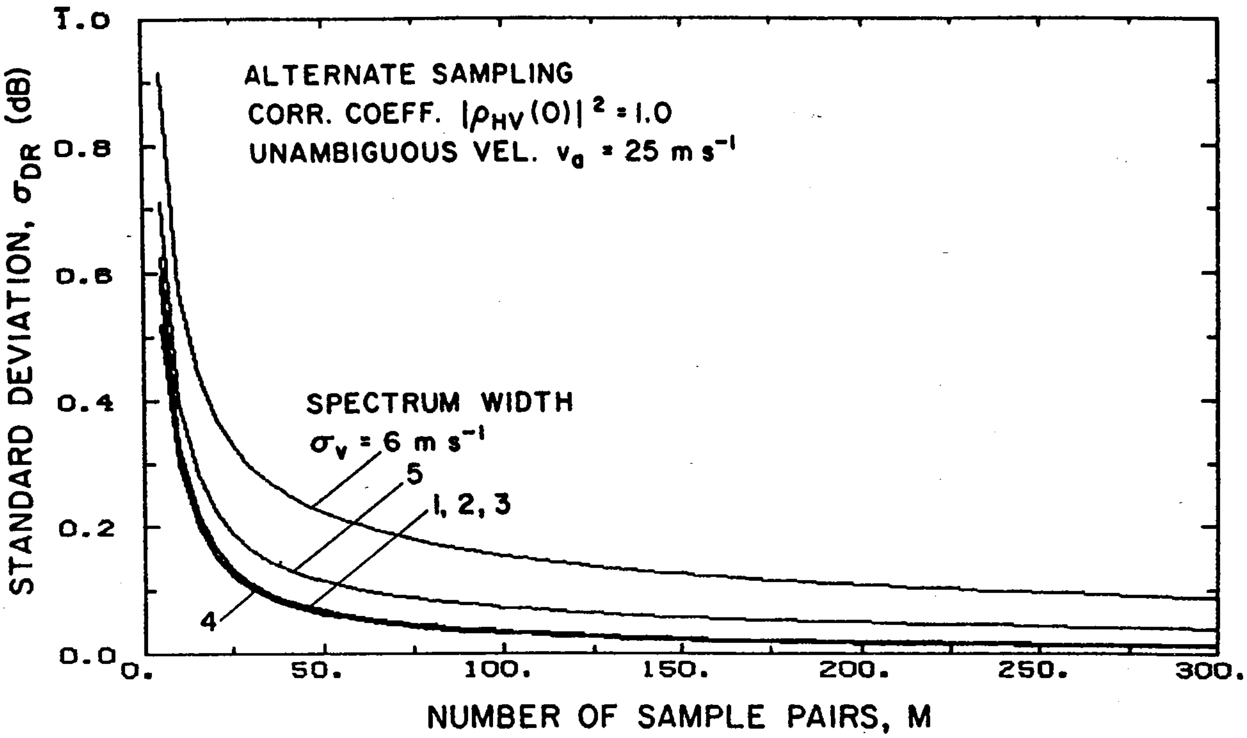

Fig. 3.1 Standard deviation of $\hat{Z}_{DR}$, σ_{DR}, versus numbers of sample pairs, M, for $|\rho_{HV}(0)|^2 = 1.0$.

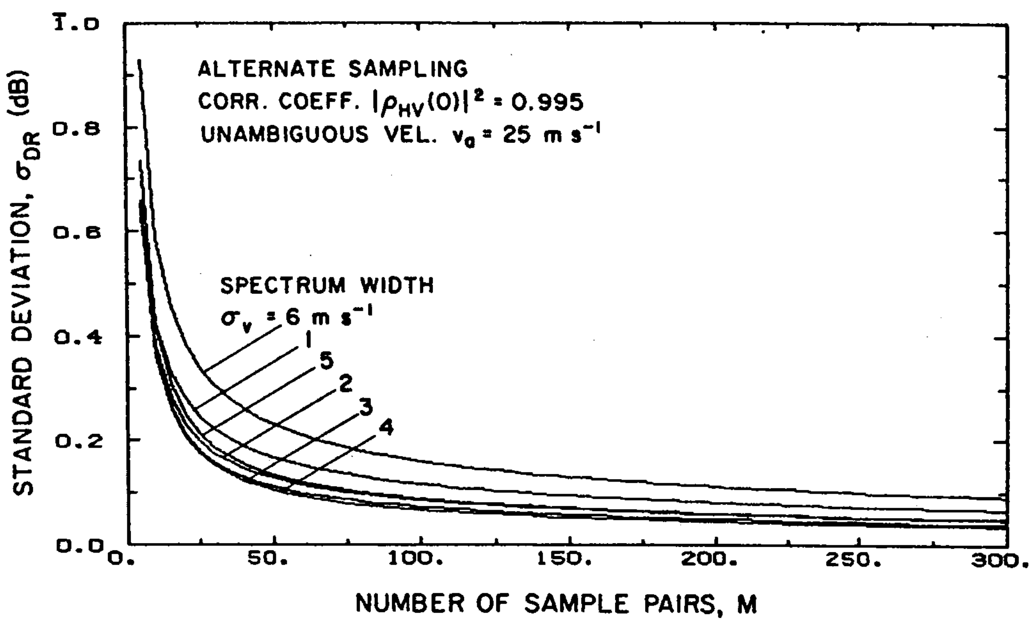

Fig. 3.2 Standard deviation of $\hat{Z}_{DR}$, σ_{DR}, versus numbers of sample pairs, M, for $|\rho_{HV}(0)|^2 = 0.995$.

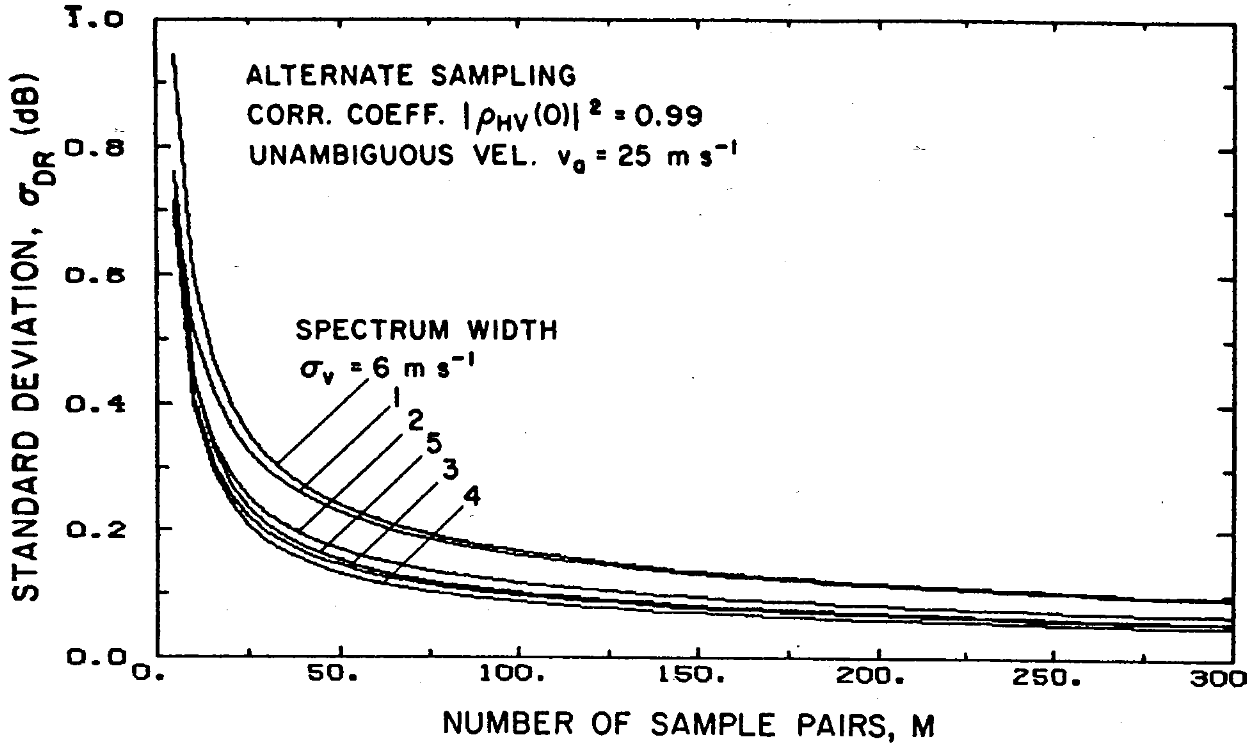

Fig. 3.3 Standard deviation of $\hat{Z}_{DR}$, σ_{DR}, versus numbers of sample pairs, M, for $|\rho_{HV}(0)|^2 = 0.99$.

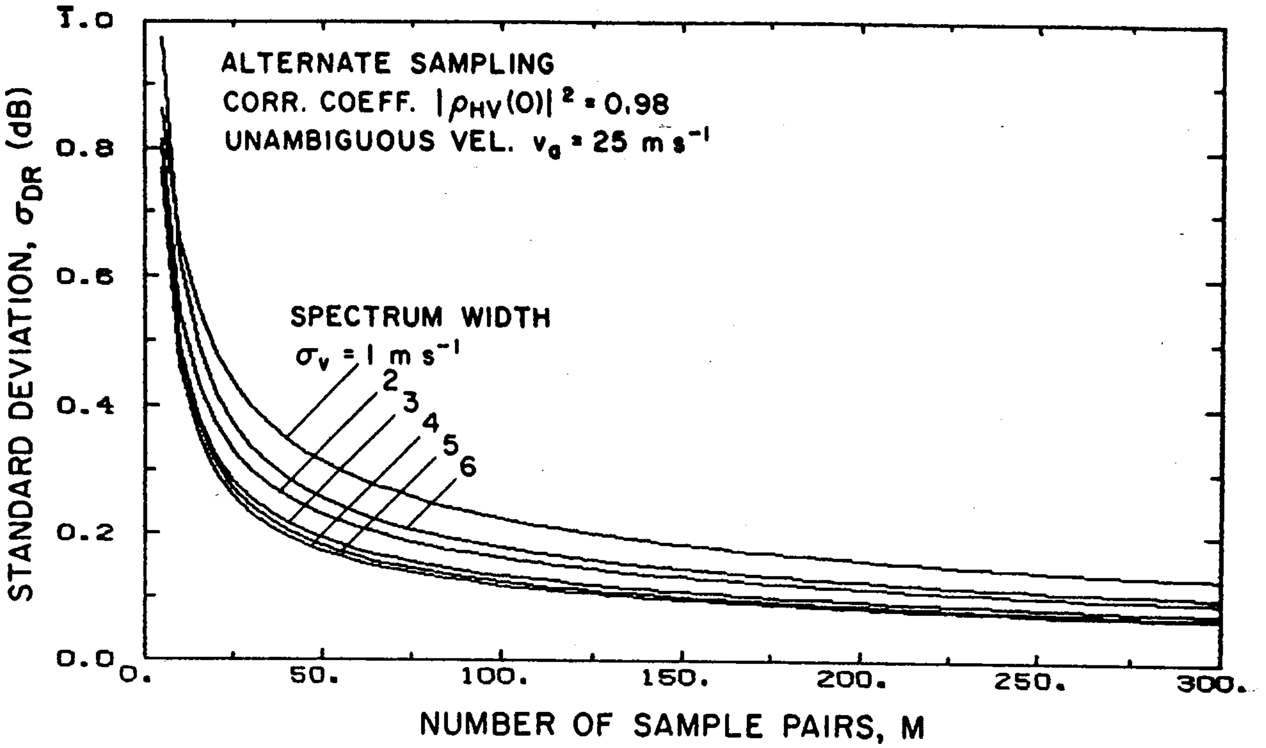

Fig. 3.4 Standard deviation of $\hat{Z}_{DR}$, σ_{DR} versus numbers of sample pairs, M, for $|\rho_{HV}(0)|^2 = 0.98$.

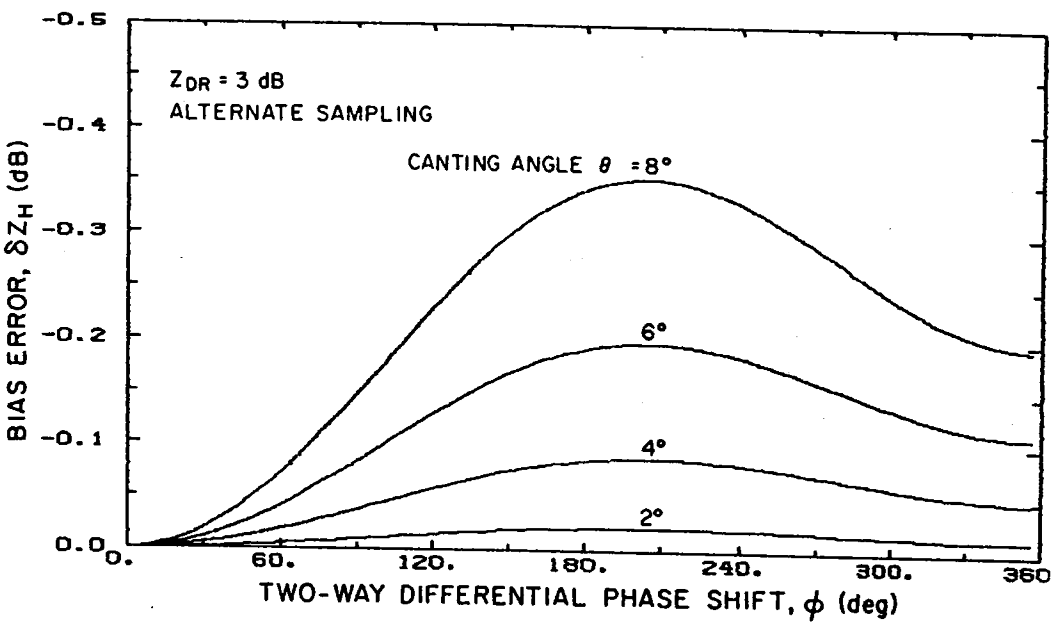

Fig. 3.5 Bias error in horizontal reflectivity, δZ_H, due to propagation with alternate sampling scheme.

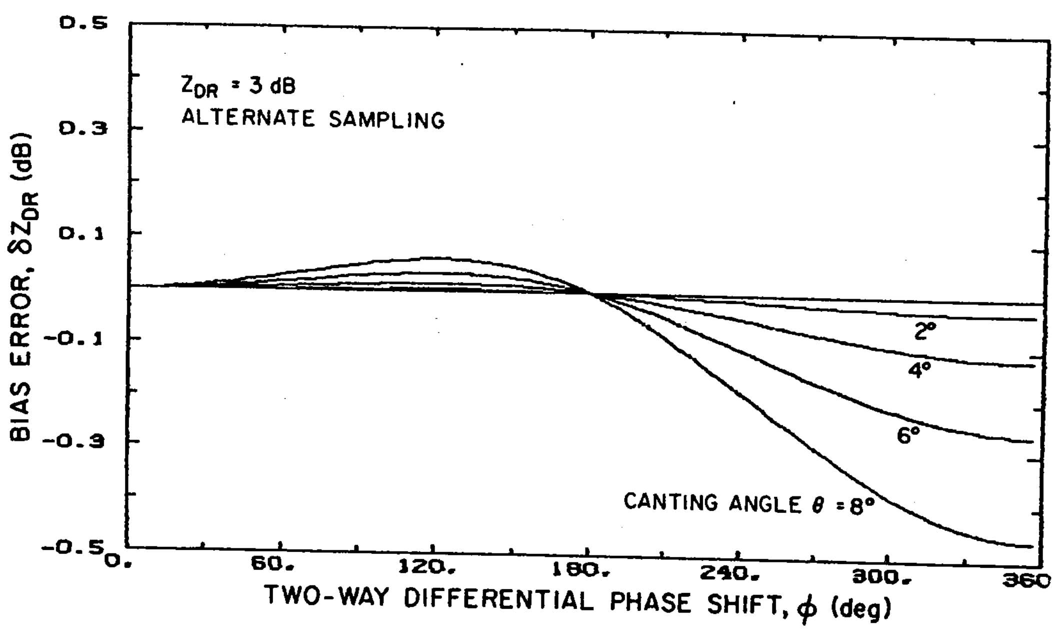

Fig. 3.6 Bias error in differential reflectivity, δZ_{DR}, due to propagation with alternate sampling scheme.

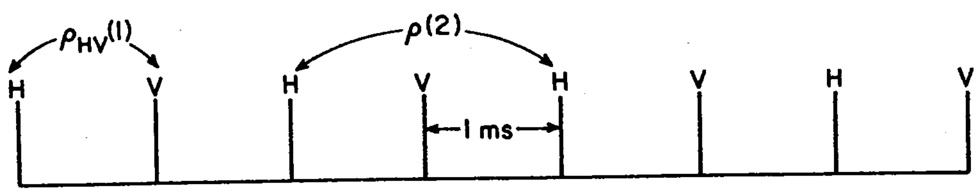

Fig. 3.7 Alternate transmission sequence. Correlations of interest are indicated.

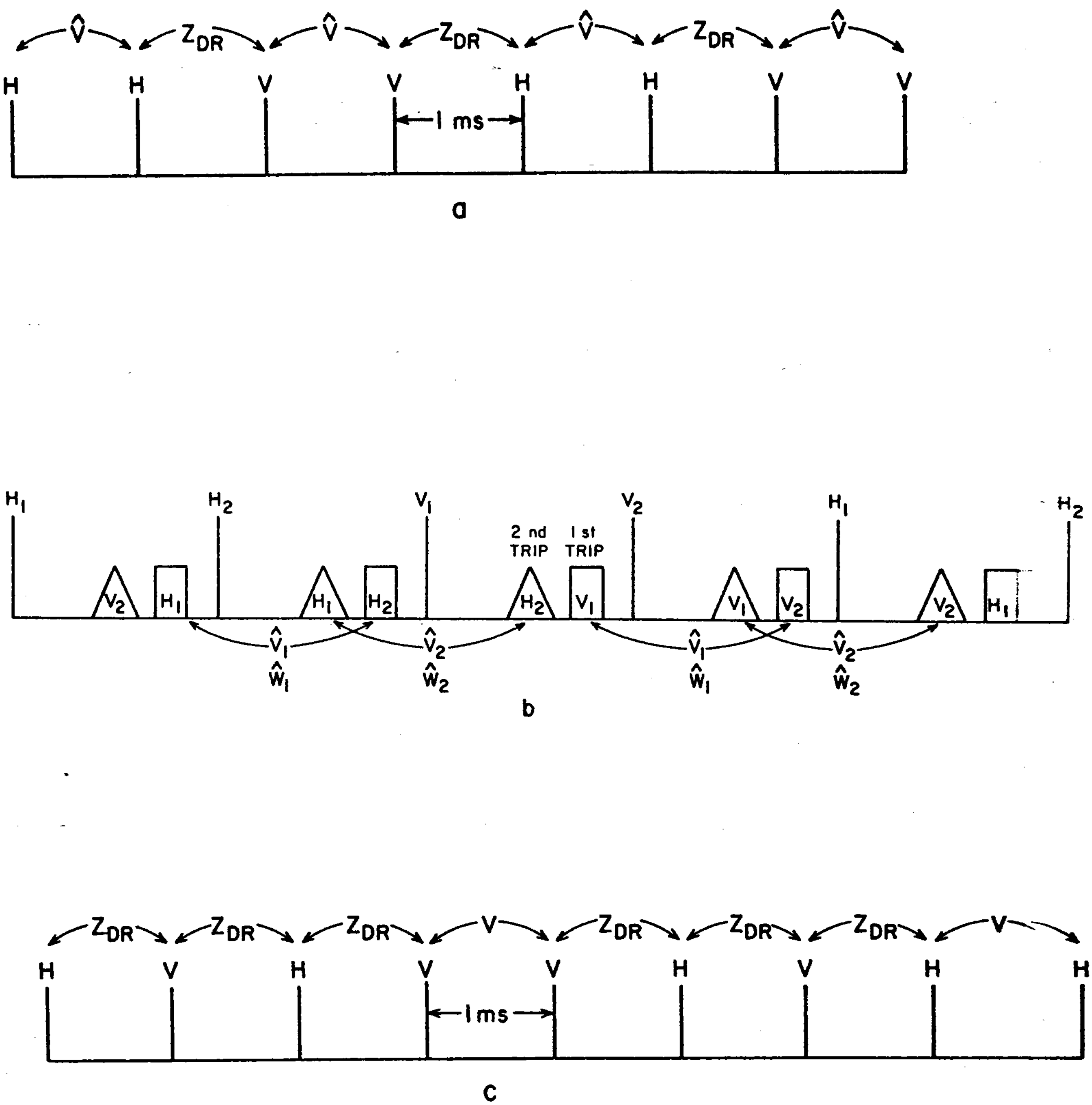

Fig. 3.8 Possible transmission sequences for NEXRAD.

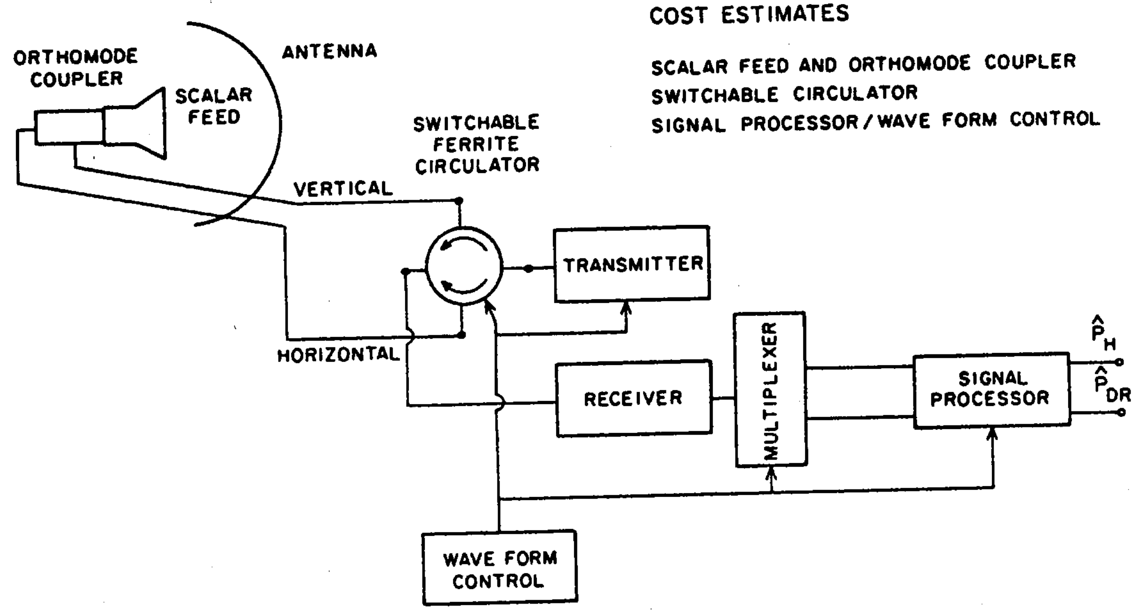

COST ESTIMATES

SCALAR FEED AND ORTHOMODE COUPLER	$5K
SWITCHABLE CIRCULATOR	$30K
SIGNAL PROCESSOR/WAVE FORM CONTROL	$20K

Fig. 3.9 Block diagram of the dual linear polarized radar for Z_{DR} measurement by alternate sampling of E_H and E_V signals.

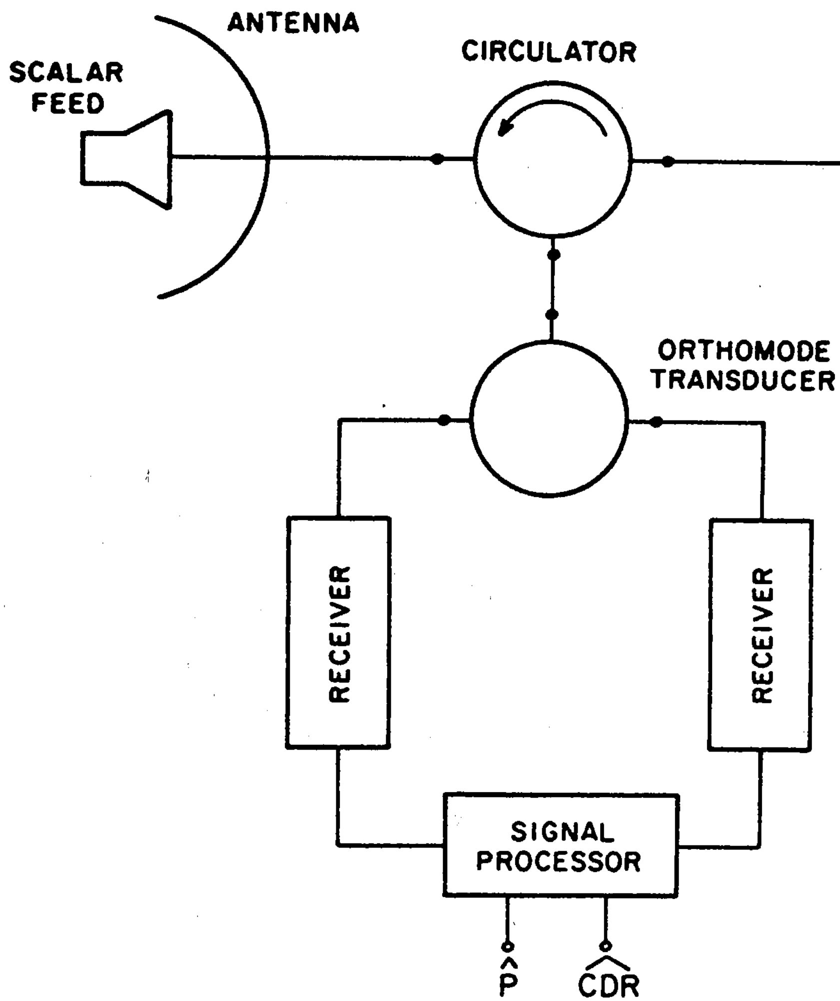

COST ESTIMATES

SCALAR FEED	$5 K
CIRCULAR/ORTHOMODE TRANSDUCER	$20 K
RECEIVER	$5 K
SIGNAL PROCESSOR	$20 K

Fig. 3.10 Block diagram of the circular polarized radar for CDR measurement.

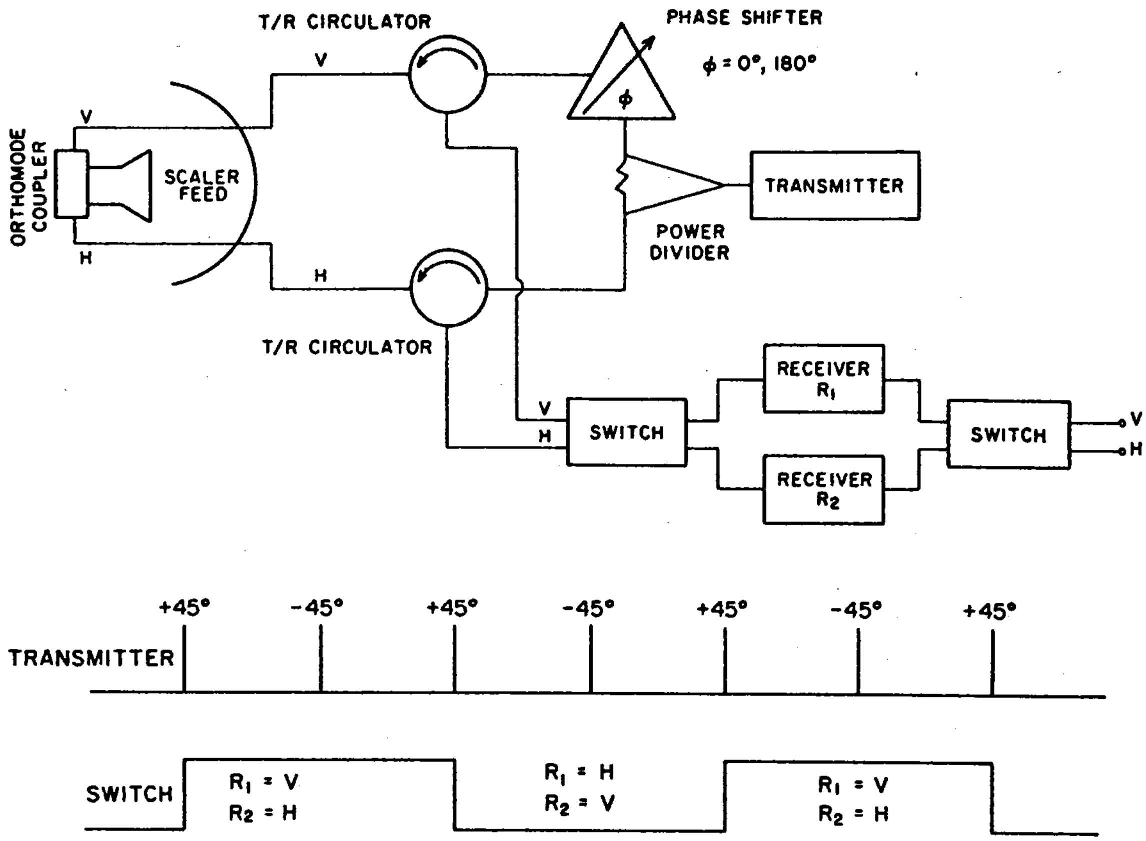

Fig. 3.11 Block diagram of radar system for Z_{DR} measurement by simultaneous sampling of E_H and E_V.

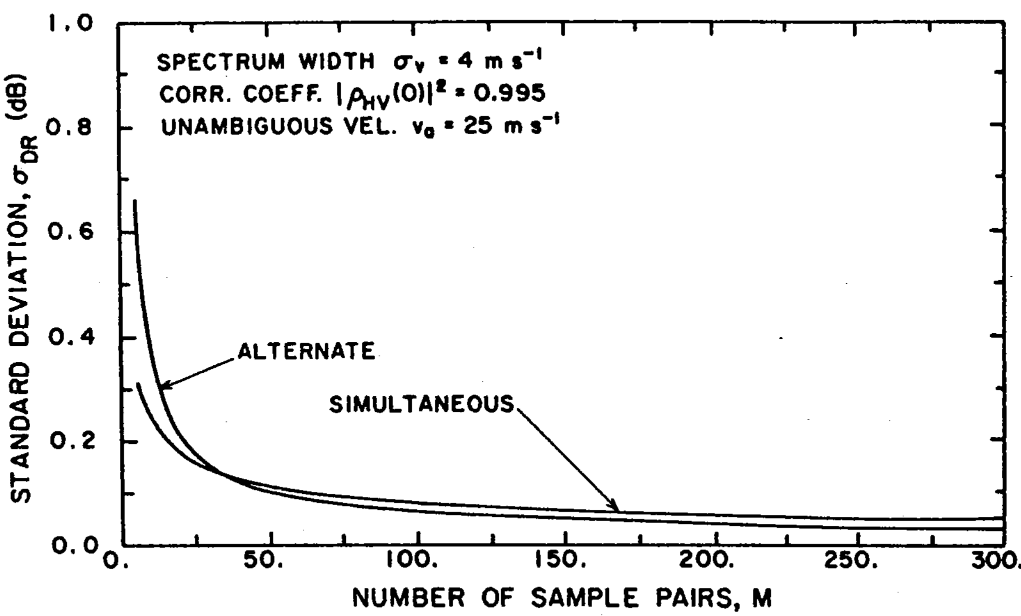

Fig. 3.12 Standard deviations of differential reflectivity, σ_{DR}, with simultaneous and alternate sampling.

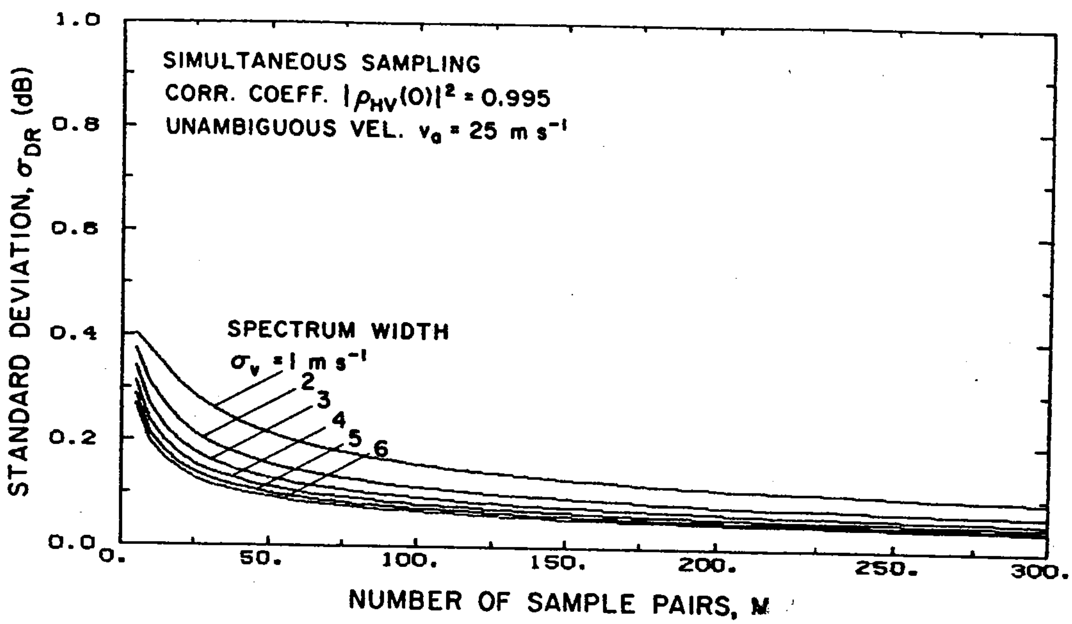

Fig. A.1 Standard deviation, σ_{DR}, versus number of pairs, M, for simultaneous sampling of E_H and E_V, $|\rho_{HV}(0)|^2 = 0.995$.

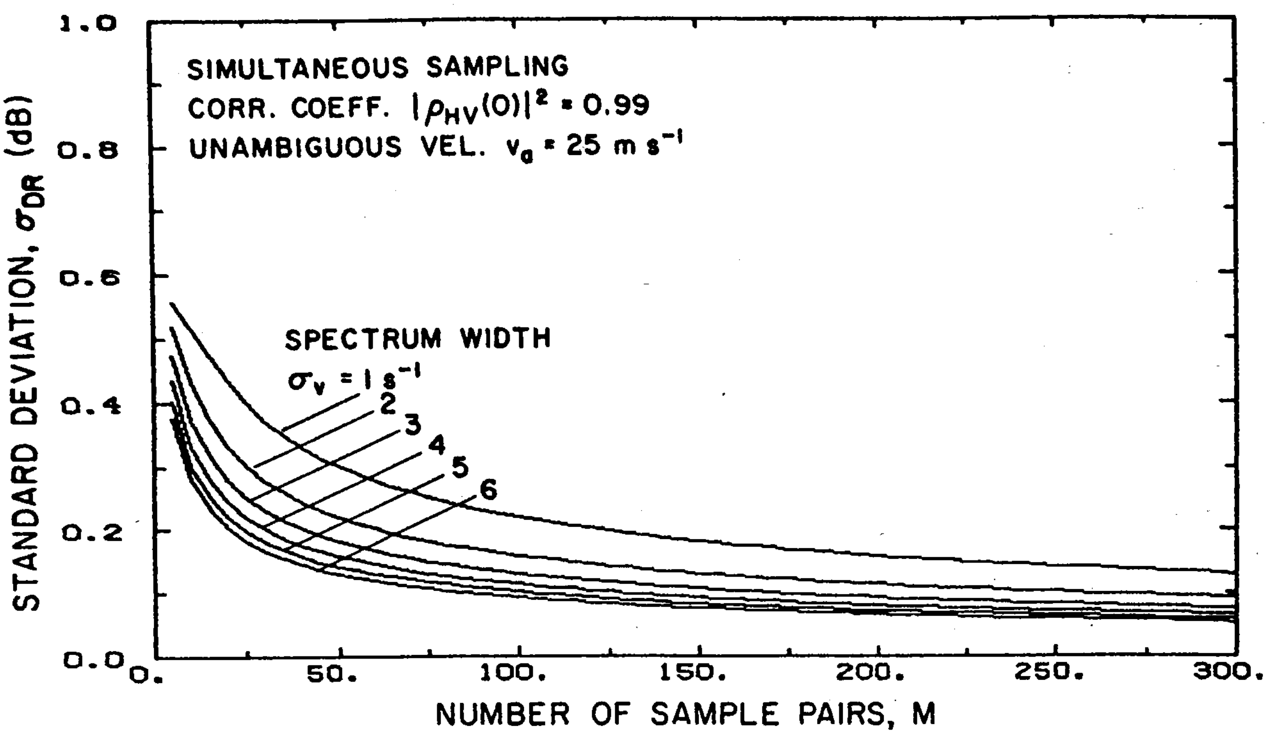

Fig. A.2 Standard deviation, σ_{DR}, versus M for simultaneous sampling of E_H and E_V, $|\rho_{HV}(0)|^2 = 0.99$.

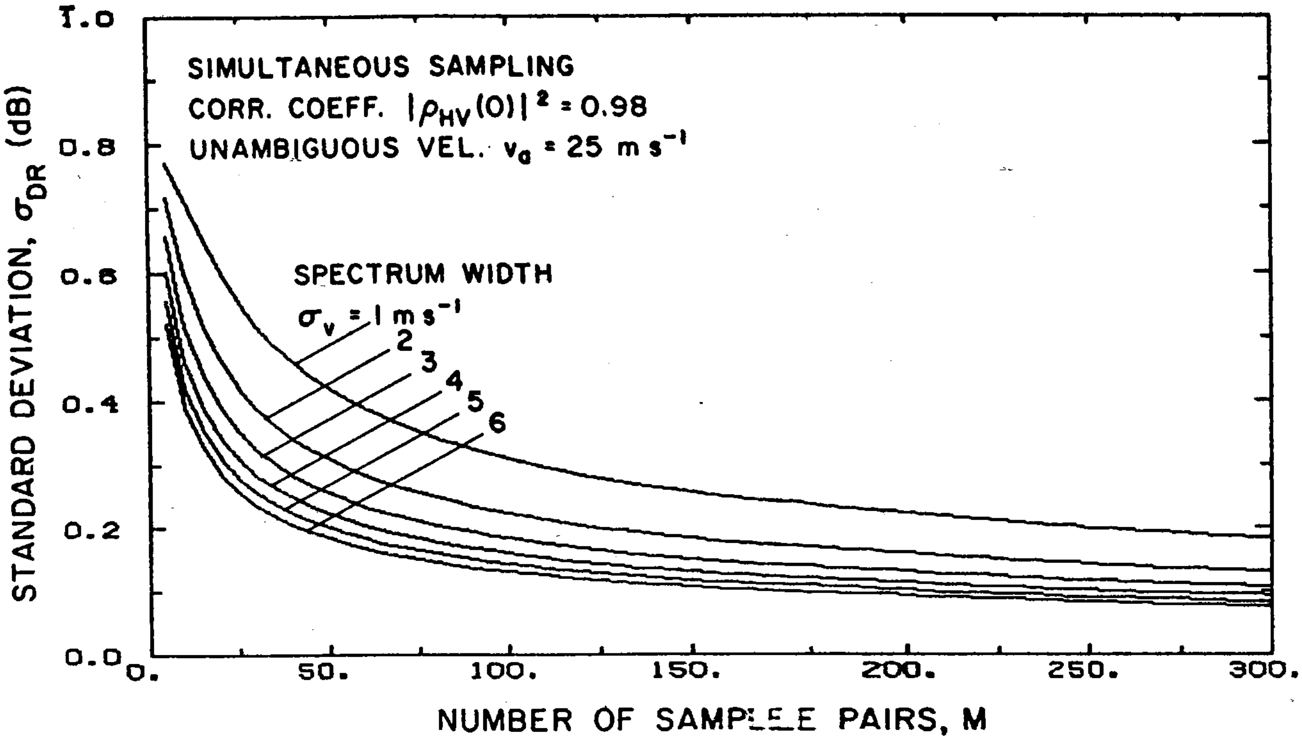

Fig. A.3 Standard deviation, σ_{DR}, versus M foror simultaneous sampling of E_H and E_V, $|\rho_{HV}(0)|^2 = 0.98$.

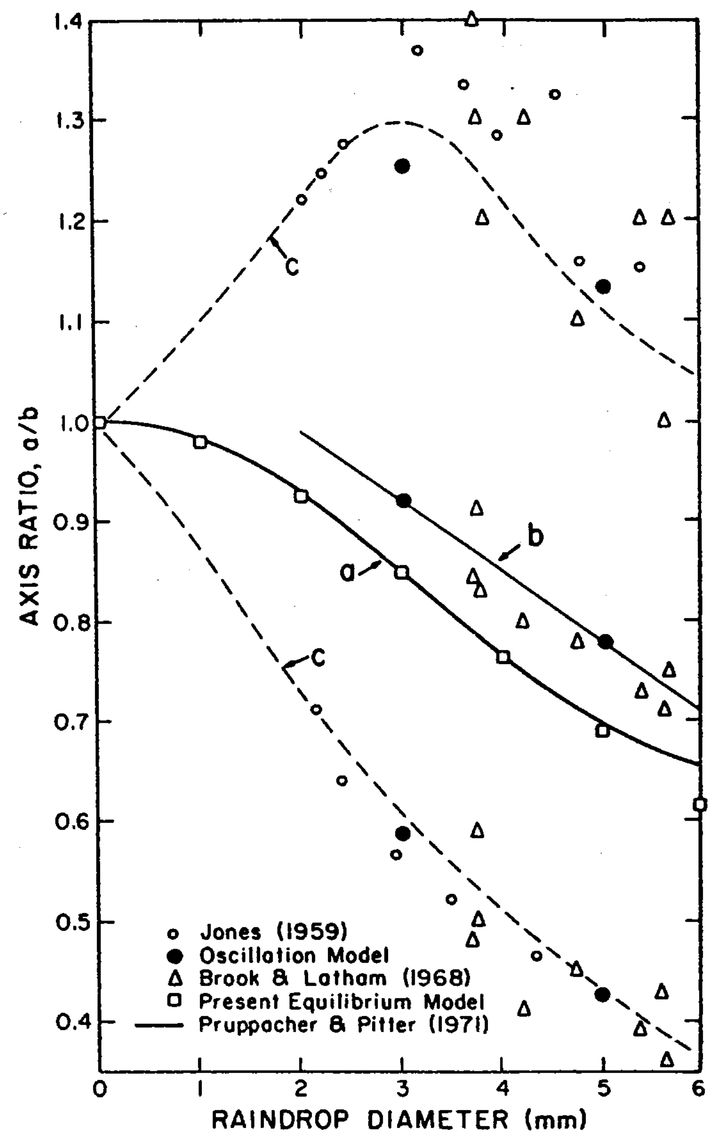

Fig. A.4 Axis ratio a/b versus equivolumetric drop diameter D_e.
(a) Equilibrium shape, (b) time averaged a/b for oscillating drops,
(c) upper and lower limits of a/b for oscillating drops.

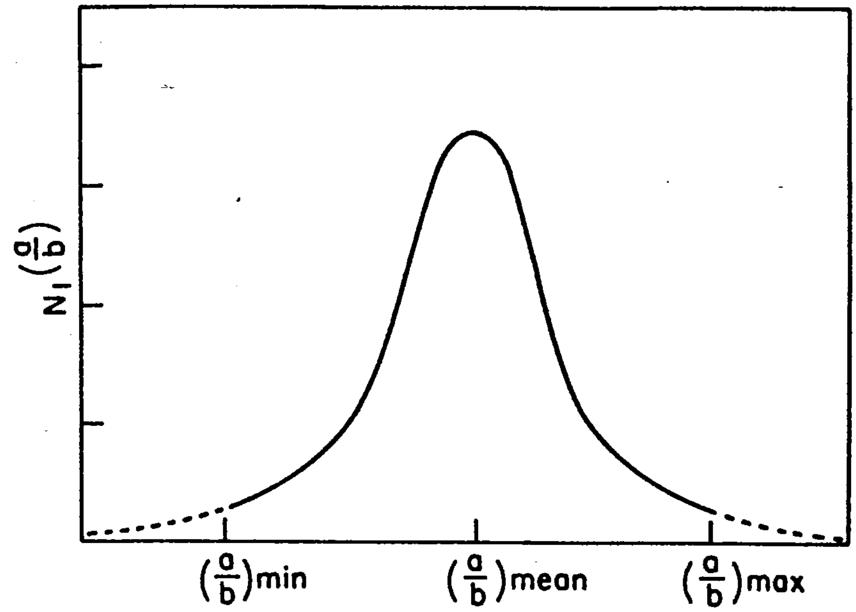

Fig. A.5 Truncated Gaussian distribution of a/b ratios.

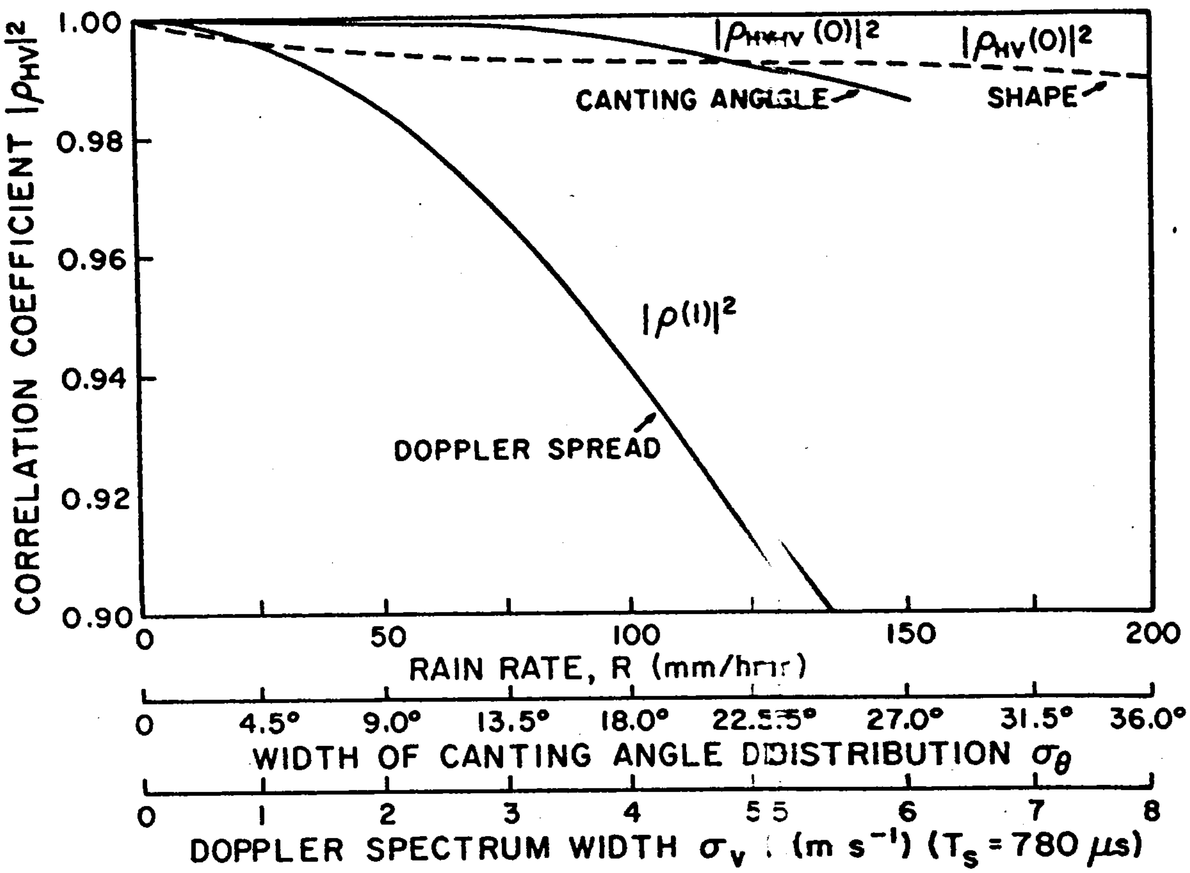

Fig. A.6 Pair correlation coefficient variation with rainfall rate R for oscillation model; standard deviation σ_θ of canting angle distribution; variation of $|\rho(1)|^2$ with spectrum width.

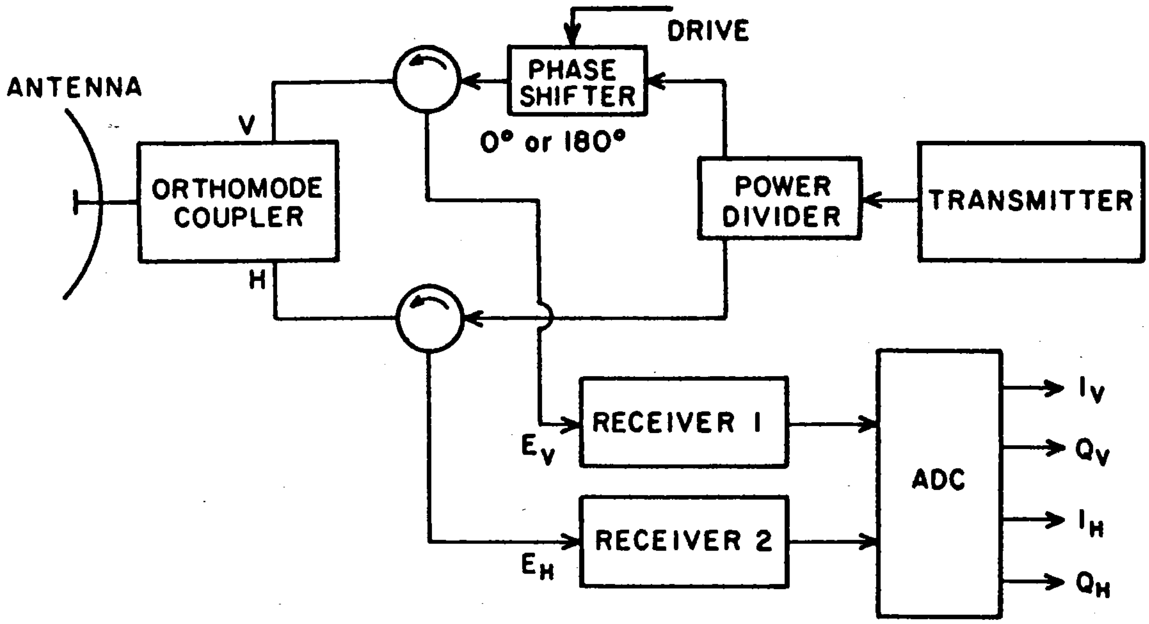

Fig. A.7 Block diagram of radar for simultaneous sampling of E_H and E_V.

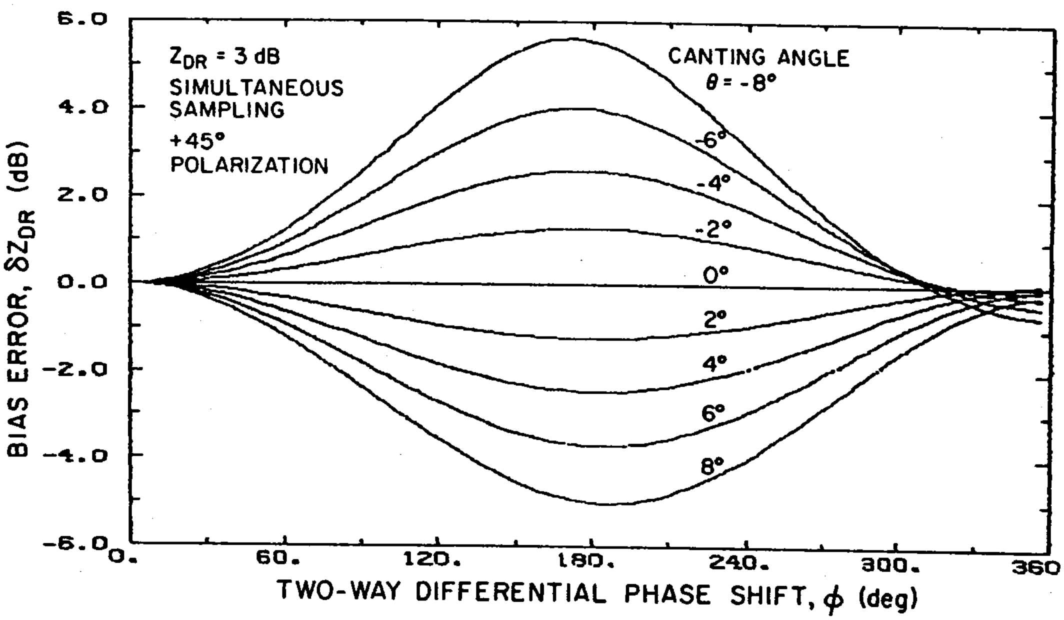

Fig. A.8 Bias error δZ_{DR} variation with two way differential propagation phase shift ϕ for transmission at +45° polarization and simultaneousus sampling of E_H and E_V. Mean canting angle θ is shown as a parameter. True value of Z_{DR} is 3 dB.

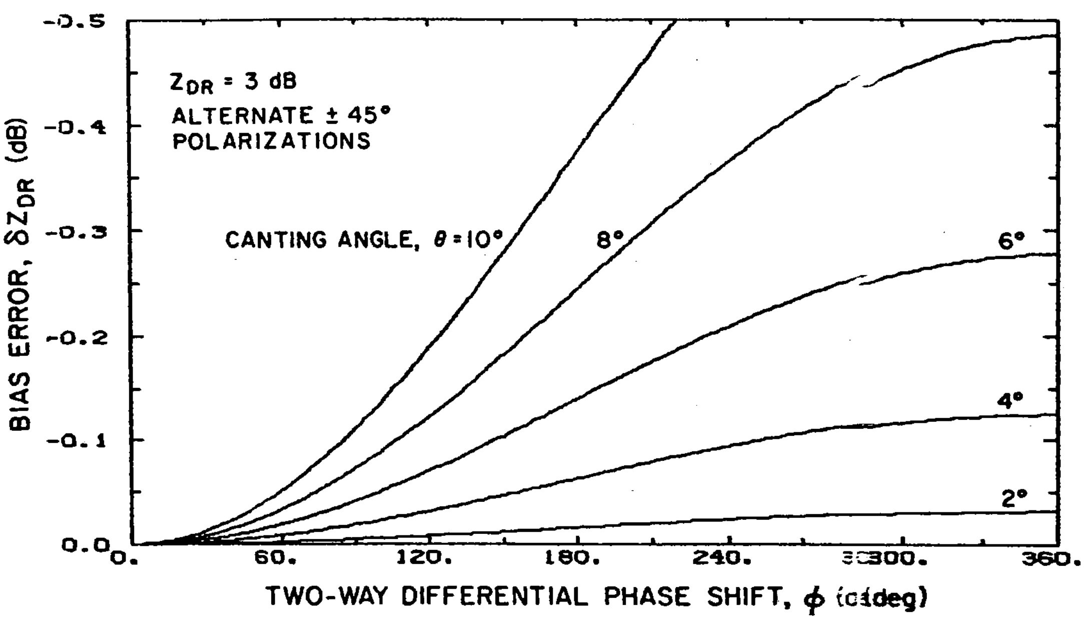

Fig. A.9 Bias error δZ_{DR} after compensation. Transmission is switched between ±45° polarizations alternately; Z_{DR} = = 3dB.

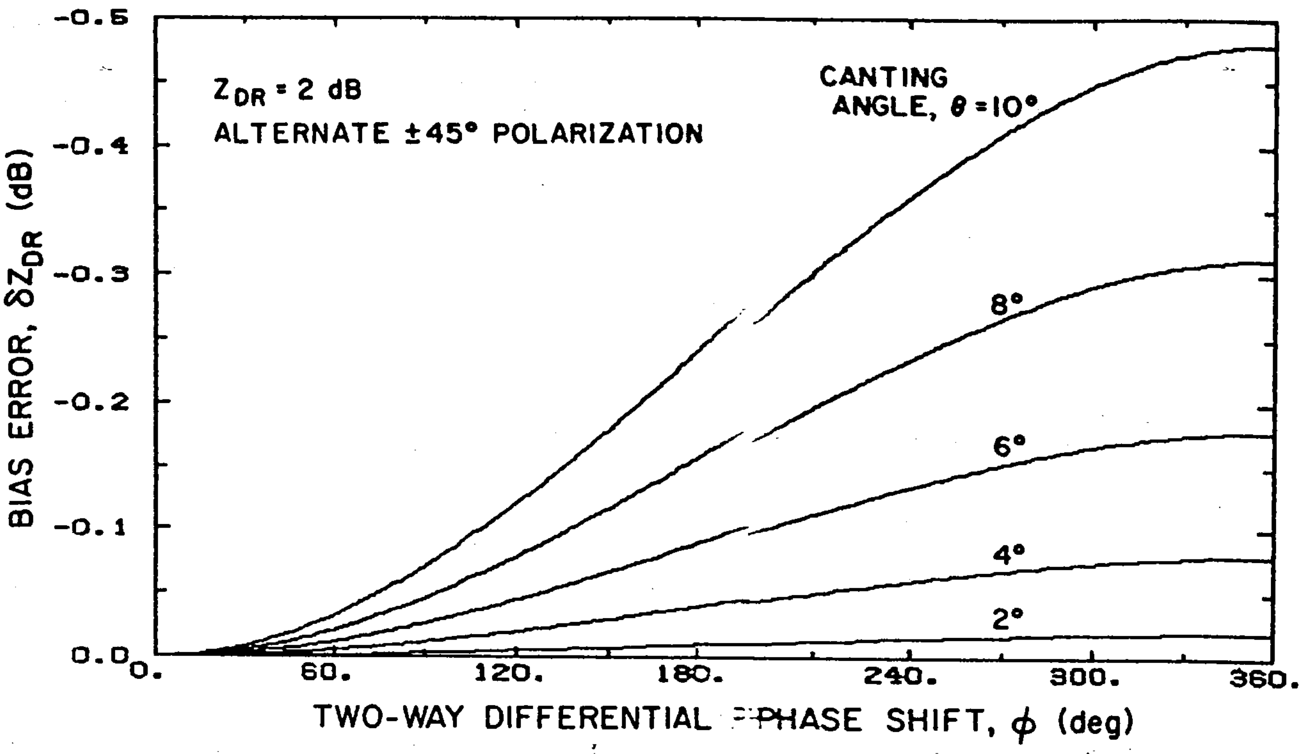

Fig. A.10 δZ_{DR} versus ϕ after compensation; Z_{DR} = 2 dB.

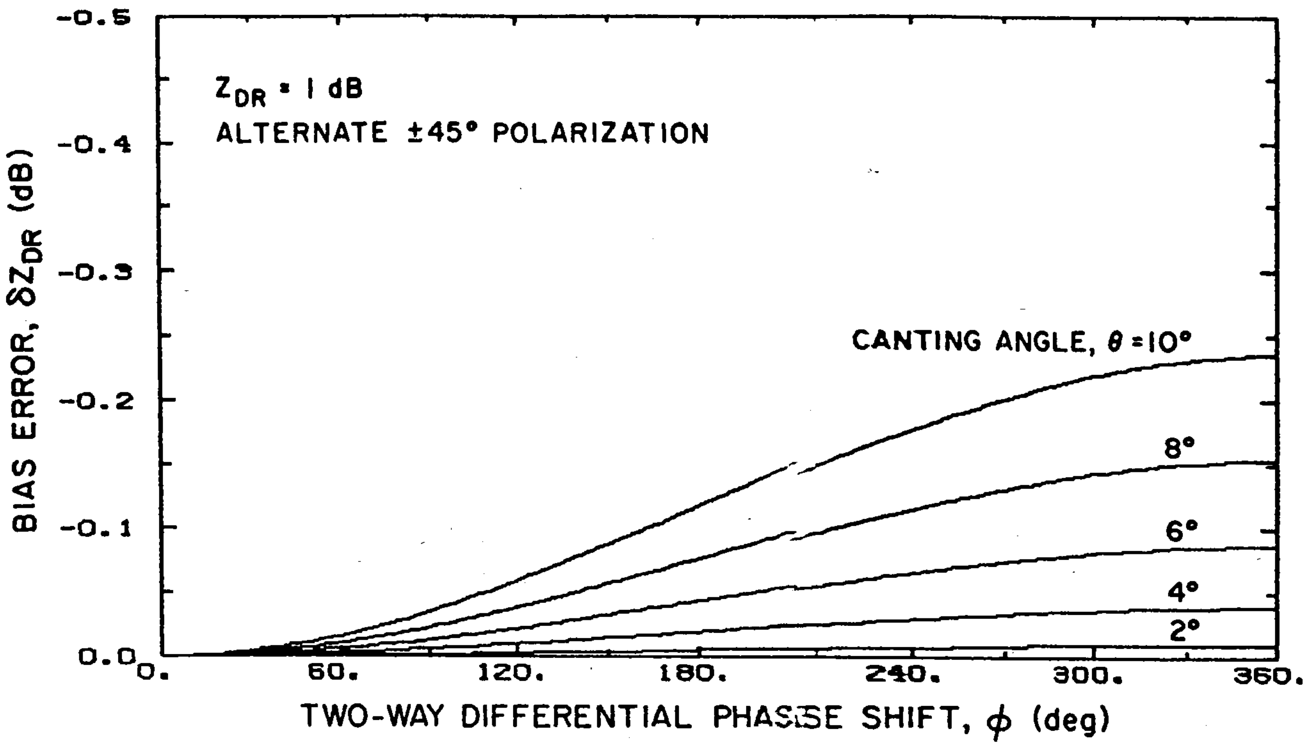

Fig. A.11 δZ_{DR} versus ϕ after compensasation; Z_{DR} = 1 dB.

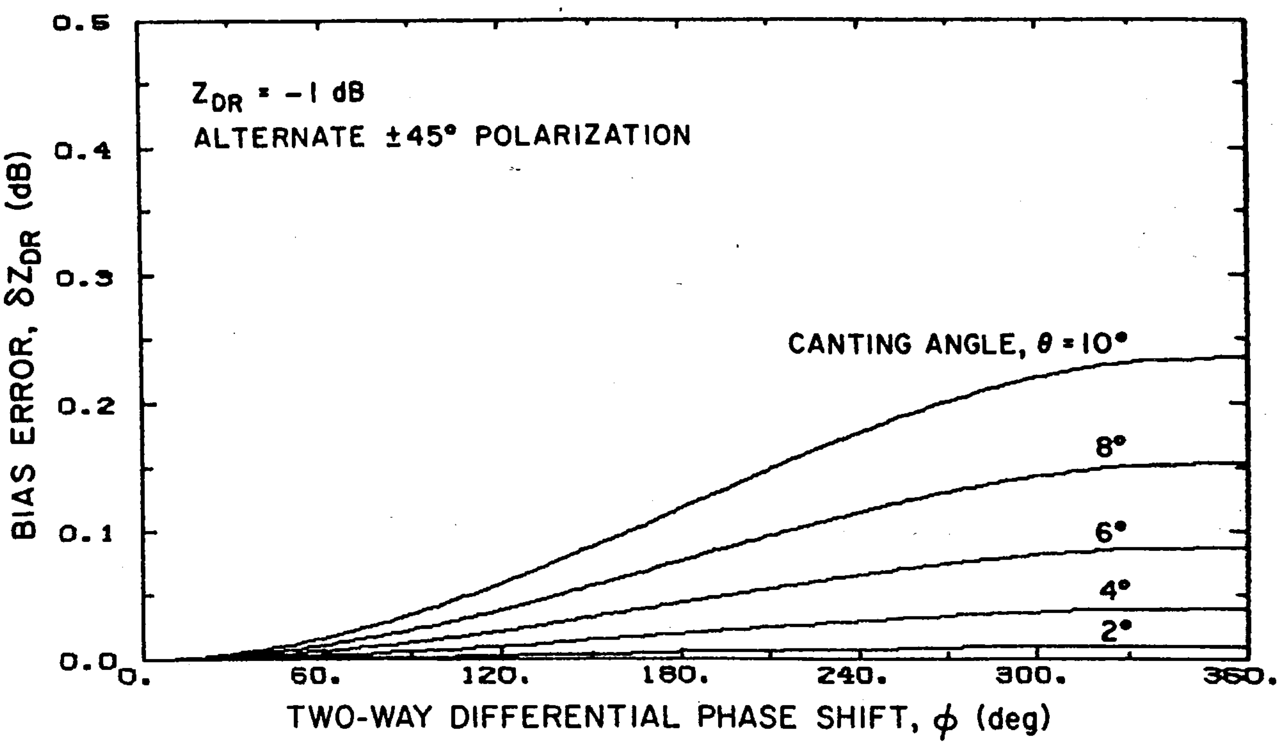

Fig. A.12 δZ_{DR} versus ϕ after compensation; Z_{DR} = -1 dB.

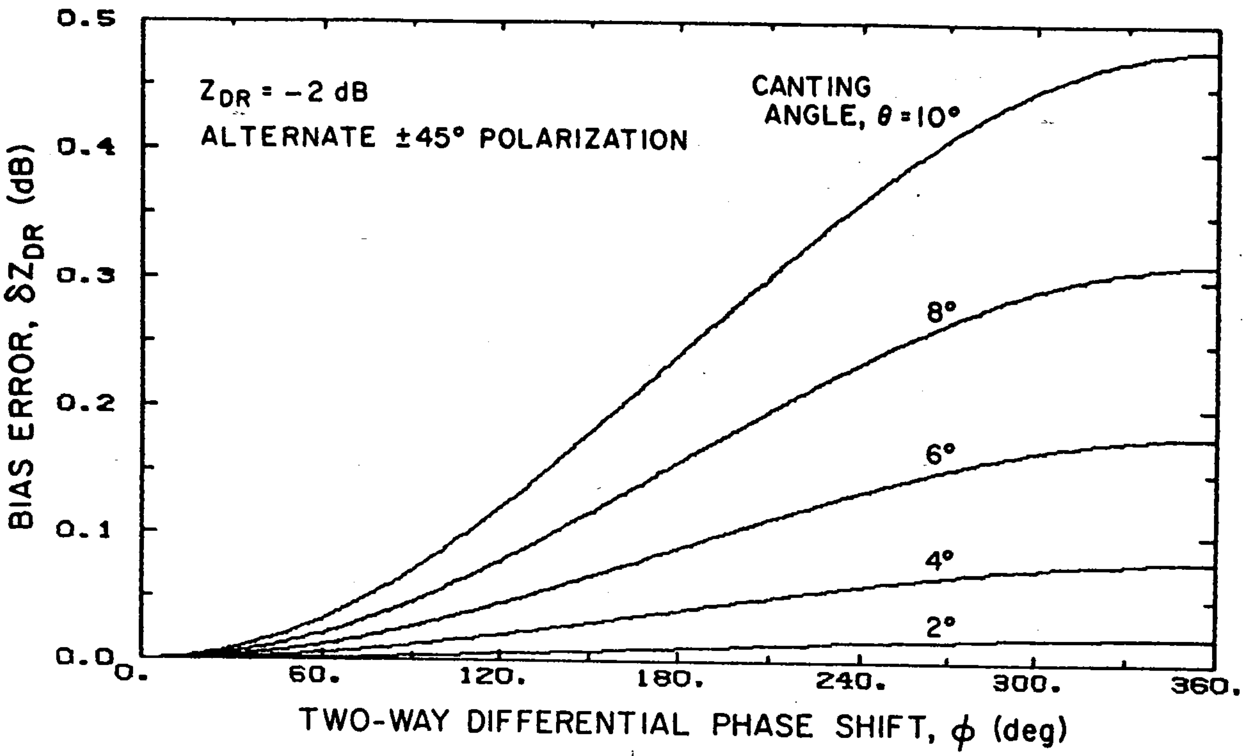

Fig. A.13 δZ_{DR} versus ϕ after compensation; Z_{DR} = -2 dB.

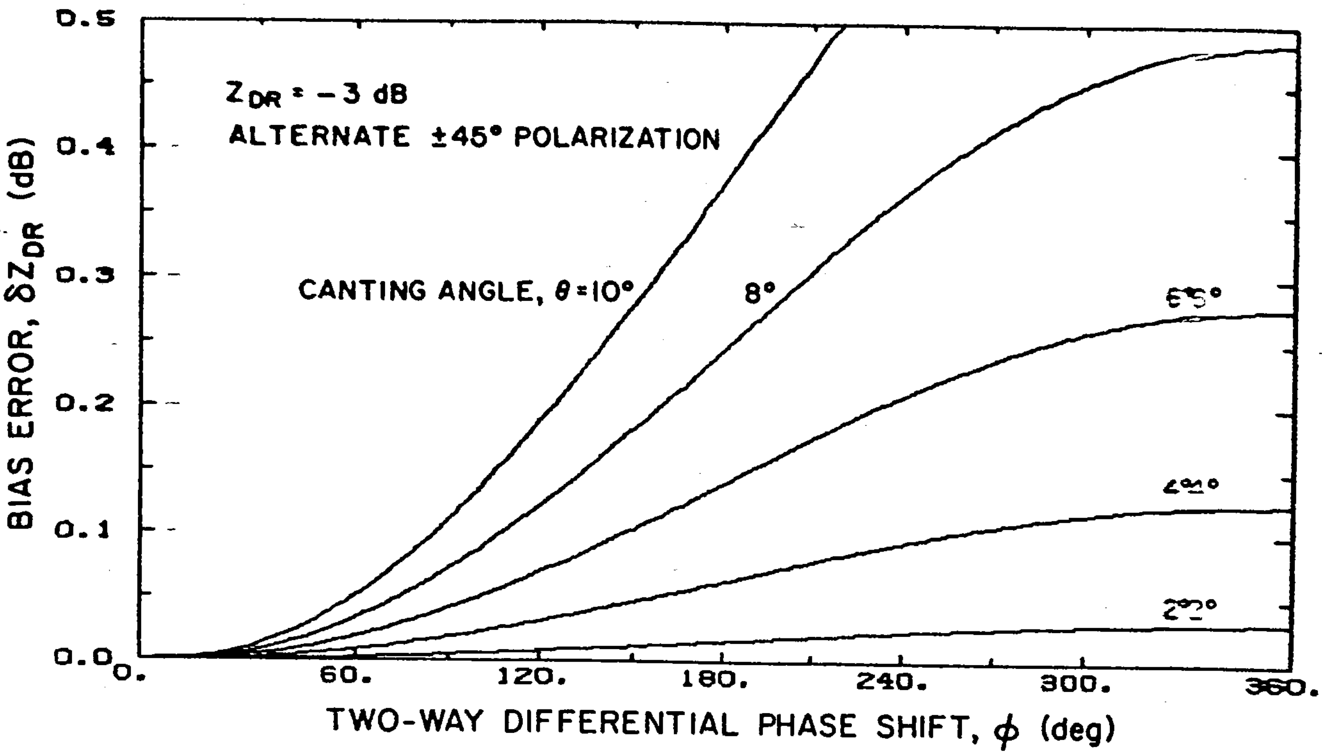

Fig. A.14 δZ_{DR} versus ϕ after compensation; Z_{DR} = −3 dB.

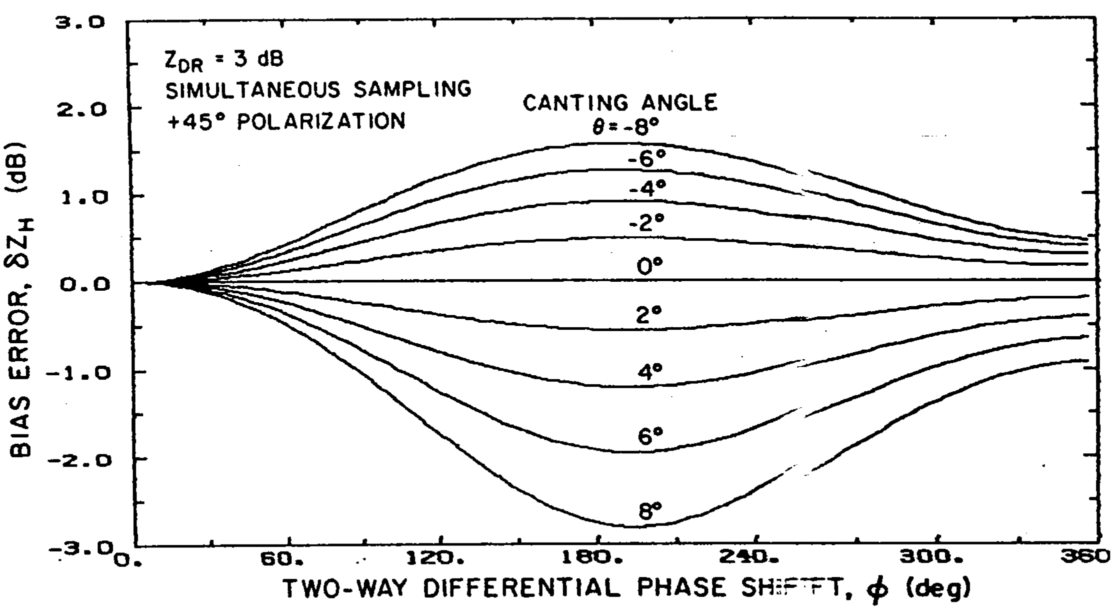

Fig. A.15 Bias error δZ_H versus two way propagation phase shift ϕ with θ as a parameter for +45° polarized transmission; Z_{DR} = 3 dB.

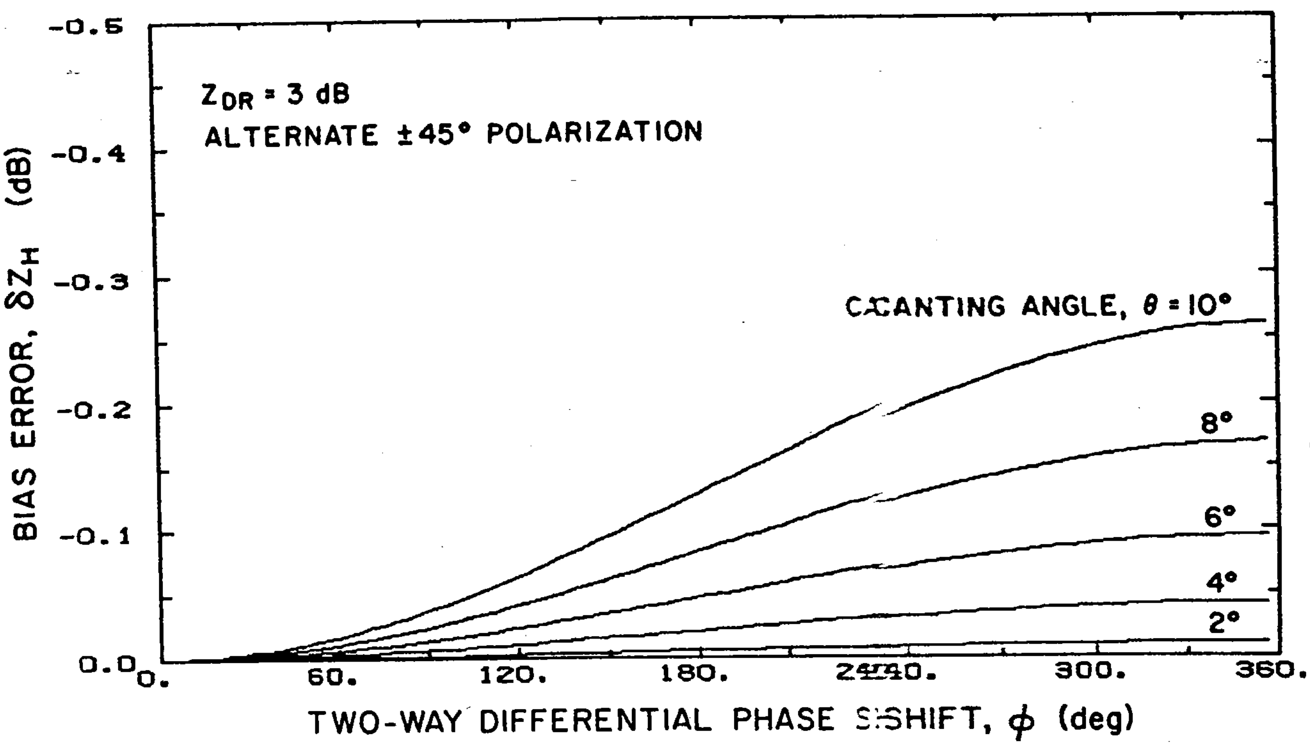

Fig. A.16 Bias error δZ_H versus ϕ after compensation; ±45° polarized transmission; Z_{DR} = 3 dB.

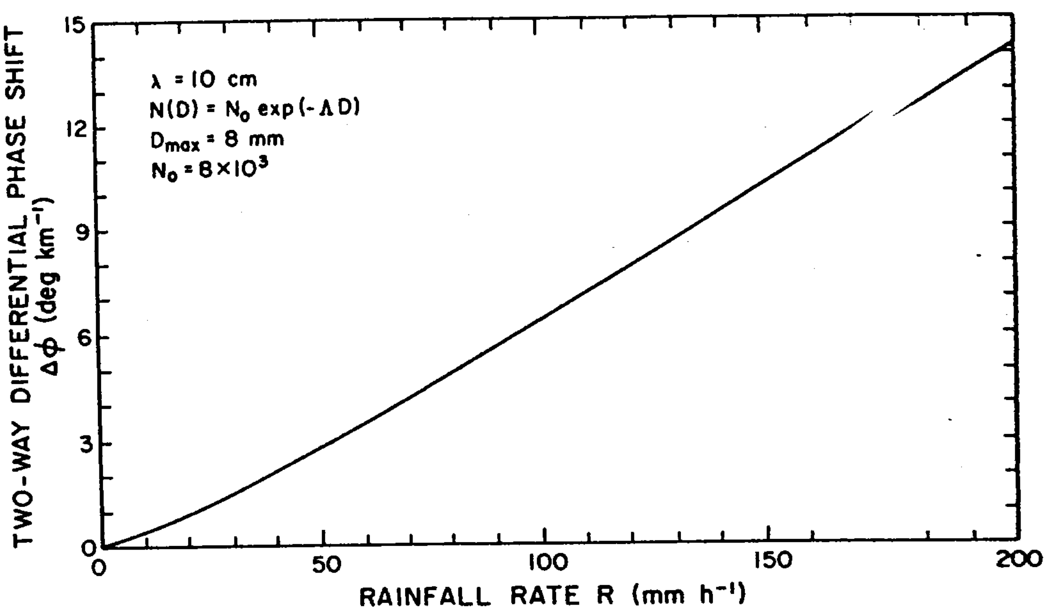

Fig. A.17 Two way differential phase shift per km versus rainfall rate R.

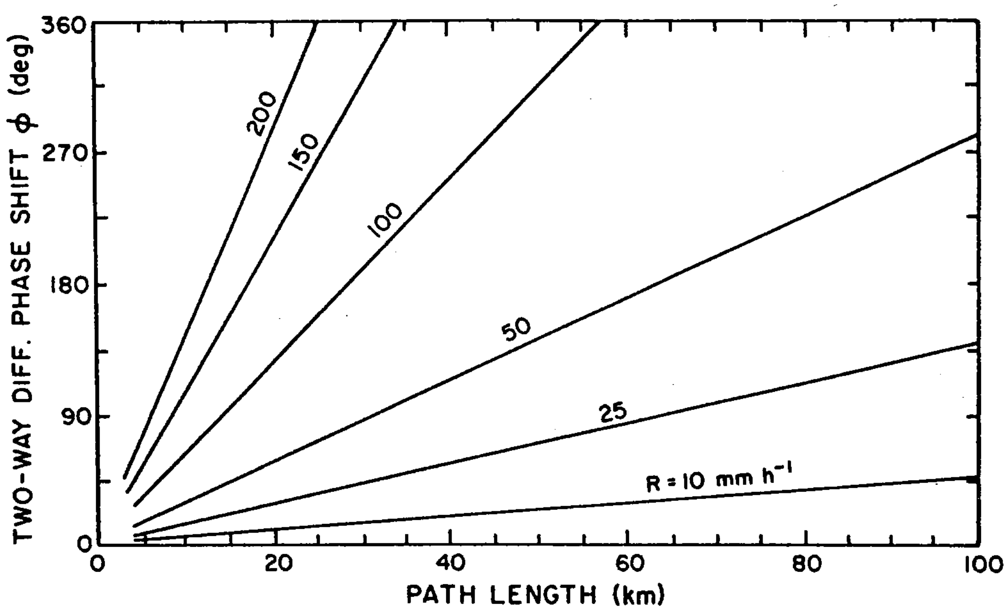

Fig. A.18 Two way differential phase shift ϕ versus path length z with R as a parameter.

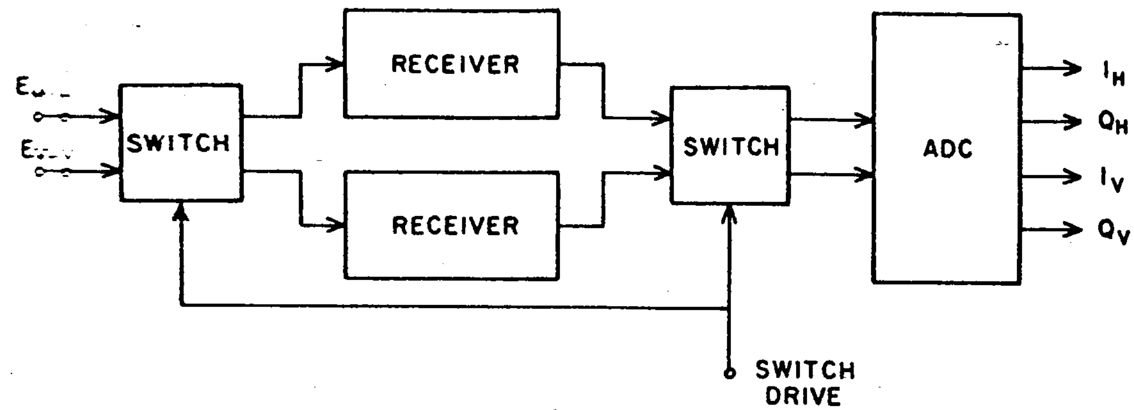

Fig. A.19 Schematic of receiver switching for mismatch compensation.

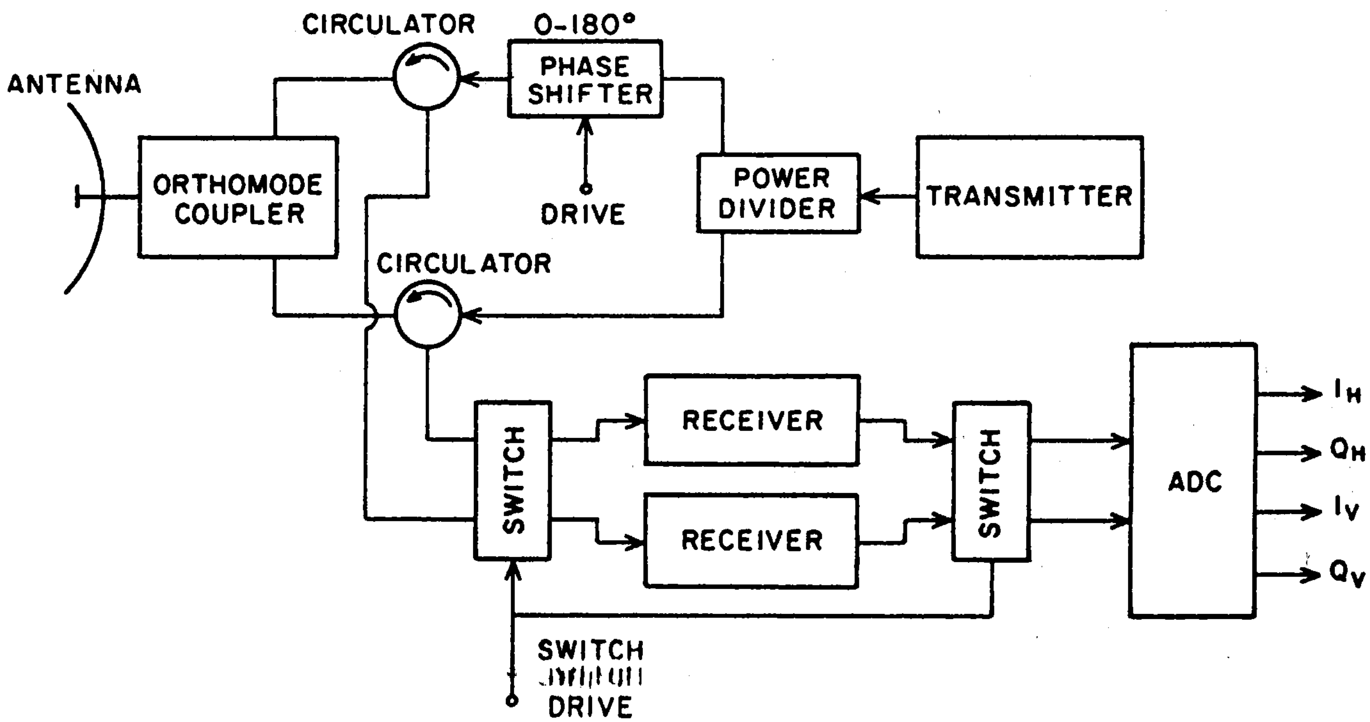

Fig. A.20 Block diagram of a radar with receiver switching.